Satellite Swarm Sensor NETwork

D1.2-S3NET Technical and Operational requirements and use case report

Project	S3NET-H2020-687351			
Deliverable N°	D1.2			
Deliverable leader	Rolf Scheiber (DLR)			
Contributor(s)	Riccardo Freddi (CGS), Eviatar Edlerman (Technion), Jamin Naghmouchi (iTUBS), Ole Bischoff (DSI)			
Internal Reviewers	Harald Michalik (DSI), Ole Bischoff (DSI), Jamin Naghmouchi (iTUBS)			
Due Date (DoA)	31.10.2016	**Submission date**	18.12.2017	
Dissemination level	CO (CONFIDENTIAL, restricted under conditions set out in MGA)			
	PU (PUBLIC, fully open, e.g. web)			X
Type	R (Document, report excluding the periodic and final reports)			x
	DEM (Demonstrator, pilot, prototype, plan designs)			
	DEC (Websites, patents filing, press & media actions, videos,etc.)			
	OTHER (Software, technical diagram, etc.)			

Table of Contents

Table of figures

Table of Tables

List of acronyms/ abbreviations used in this document

Acronym/ abbreviation	Definition
BLU	Best Linear Unbiased
CCSDS	Consultative Committee for Space Data Systems
CLD	Central Local Difference
DDGPS	Double Differential GPS carrier phase processing
DLD	Directional Local Difference
EOK	Extended Omega-K algorithm
FLOP	Floating Point Operation
FLOPS	Floating Point Operations per Second
IRF	Impulse Response Function
PR	Prediction Residual
PRF	Pulse Repetition Frequency
PRI	Pulse Repetition Interval
SAAB	Space Applications Advisory Board
SAR	Synthetic Aperture Radar
SVM	Support Vector Machine
TSX	TerraSAR-X
TDX	TanDEM-X

1 EXECUTIVE SUMMARY

This technical note describes a pre-selection of optical and radar use cases, which are expected to benefit from improved on-board processing and communication performance as will be developed within the S3NET study. Special attention is given to those applications requiring a distributed or fragmented system with sensors flying in close formation.

The identified applications for optical remote sensing are cloud detection and image compression, both being beneficial for reducing of the amount data for downlink, as well as band registration for the spatial alignment of spectral channels. Fractionation is proposed either for enlarging the observed region or for increasing the number of spectral channels.

The two pre-selected radar applications relate to the Tandem-L mission proposal and to a bistatic formation to enhance observation capabilities of a potential future Sentinel-1 follow-on mission. For Tandem-L the staggered SAR operating mode is foreseen to avoid blind regions across the imaged swath. Its on-board processing approach for low-pass Doppler filtering and decimation is identified as potentially benefitting from the S3NET development. Concerning the bistatic formation, the SAR image formation is primarily investigated in this report, supplemented by synchronisation processing and data reduction aspects by means of multi-looking.

The report also includes a detailed assessment concerning the feasibility of (autonomous) formation flying for the bistatic radar mission. A similar methodology will be applied to the optical case during the mission analysis study to be conducted within the next phase of the project.

Computational and communication requirements are evaluated in detail for all investigated use cases to allow the selection and dimensioning of suitable hardware solutions for the S3NET on-board compute and communication simulation systems. It is found that the most demanding processing requirements are posed by the bistatic SAR image formation followed by the optical image registration processing, both requiring multi-processor DSP solutions. Inter-satellite communication requirements for the bistatic SAR case are, after this preliminary assessment, most demanding and at the limit to what X-band inter-satellite links can provide. However, taking into account different mission design alternatives, there is no strict requirement for optical laser links to be investigated within S3NET, especially as there is no constant latency requirement for the envisaged radar application.

2 INTRODUCTION

In document D1.1 of S3NET an initial requirement analysis has been performed regarding Earth observation systems carrying optical and radar sensors. In particular the benefits of operation in a formation and the requirements for on-board processing have been assessed in a qualitative way, especially with regard of service enhancement and provision of new information products. For both sensor categories a number of use cases have been identified. A representative subset for each category, which best covers the future operational needs, has been pre-selected to be investigated in more detail in a quantitative way within the present task and to allow subsequently the definition of both, the S3NET concept compute system and the S3NET communication simulation system.

For each use case we identify in this document the on-board processing requirements, establish an associated preliminary mission plan including, where applicable, first requirements for formation flying, and quantify the necessary performance for communication and data exchange with ground stations and within the formation. A preliminary benchmarking plan is established for each use case to initiate the iteration to be conducted later on within WP2, WP3, and WP4.

The follow-on sections of this technical note are structured as follows: Section 3 discusses the **pre-selected optical application** for S3NET, namely on-board cloud detection, on-board compression, and on-board band registration. These applications are further associated to two different formation flying mission scenarios which are discussed in section 3.5 and for which the communication requirements are also summarized.

The **radar use cases** are discussed in section0. In particular, four use cases are pre-selected: staggered SAR data decimation, on-board SAR image formation, bistatic synchronisation, and SAR image multi-looking. Also in this case we evaluated the computational requirements and established the demands for communication and formation flying.

Section 5 provides a first, specific assessment on the **formation flying feasibility** for the radar mission concept associated to the bistatic imaging use case. During the next phase of the project, these type of specific analysis will be deepened and similar analyses will be performed also for the optical case.

The **computational requirements** originating from the optical and radar use cases are quantified in section 6, whereas the identified **communication needs** are discussed in section 7.

Section 8 concludes the requirement investigations.

3 OPTICAL APPLICATIONS SCENARIOS

This chapter covers the activities of collecting, validating, translating and organizing downstream needs in the optical EO application scenarios.

3.1 Application selection

Within the scope of the S3NET project, a computational analysis reported in this document has been done on three image processing algorithms to be implemented on-board optical satellites. The applications of interest selected for possible real-time pre-processing were selected based on a state-of-art analysis, described in the D1.1 document. Such applications are:

- Cloud detection,
- Band-to-band co-registration (BBR), and
- Data compression.

These applications have been reputed to be extremely useful, especially for the purposes of reducing the amount of data to be downlinked from the space platform to the ground segment. This impacts positively on the space-to-ground link performances. The three applications can also benefit from each other. As matter of consequence, a BBR application is extremely important for clouds detection. In fact, better co-registration will result in better cloud classification by removing misleading "spectral mixes" between adjacent pixels. Then, a well-defined cloud boundaries map will ensure better compression of the data. Moreover, these applications have been already implemented in different earth-observation optical satellites.

As mentioned above, a deep state-of-the-art analysis has been carried out in order to select an algorithm for each application. It is done by looking at different aspects such as complexity, robustness, performances, etc. The analysis can also be reviewed in document D1.1. For the BBR application two algorithms have been proposed. The first one has been developed by (Yu, Vladimirova, & Sweeting, Autonomous band registration for on-board applications, 2007), and the second one by (Albinet, Camarero, Isnard, Poulet, & Perret, 2013). In the following only the first one will be described because it offers a clear definition of the processing steps, and it has been proved to be robust and computationally performant.

On-board cloud detection is one of the most important applications because it can help in reducing the total amount of data to be downlinked and in reducing also the amount of errors done downstream by e.g. land cover classification algorithms. In the literature, the majority of the techniques present classifications based on spectral reflectances, or on a ratio of them. In D1.1, two algorithms respectively proposed by (Camarero, Thiebaut, Dejean, & Speciel, 2010) and (Thompson, et al., 2014) have been selected. The first one has been analyzed more in details because it offers very low computational requirements, and is thus extremely well suited for operation on-board satellites.

Data compression has also been deeply analyzed, as for the two previous applications. In this case, our attention has been oriented in the 'Consultative Committee for Space Data Systems' (CCSDS) framework. The CCSDS has defined several techniques for data compression to be implemented on on-board satellites. As before, two different algorithms have been selected for this application (see

report D1.1). The two were proposed by (Klimesh, Low-complexity lossless compression of hyperspectral imagery via adaptive filtering., 2005), and (Nian, Xu, Wan, Wang, & He, 2016). They implement respectively a 'lossless' and a 'lossy' technique. The first one has been selected, and thus is described in more detail below. The 'lossless' technique has the advantage to retain all the information at the cost of a lower data compression. Moreover, (Santos, Berrojo, Moreno, J., & López, 2016) proposed an efficient FPGA architecture which can be deployed on on-board satellites.

In the next paragraphs, the algorithms will be analyzed, focusing on computational requirements. They have been split into elementary blocks and, for each of them it has been reckoned the required amount of Floating-point Operations (FLOPs). A FLOP is assumed to be either a complex multiplication or a complex summation as defined in (Hunger, 2007). Finally, the algorithms have been analyzed by using the Sentinel-2 characteristics in an example computation. This has been done in order to get a reliable reference term to coarsely evaluate the complexity and the maximum number of FLOPs required on-board the satellite. As expected, the processing time is mostly related to the FPGAs and their capability in terms of FLOPs per second. Furthermore, efficient parallelization, where possible, will increase performances, and thus reduce the processing time.

3.2 On-board cloud detection

The selected cloud detection algorithm is based on Support Vector Machine techniques (SVM) classification. As already mentioned, the method was proposed by (Camarero, Thiebaut, Dejean, & Speciel, 2010). The main stages of the algorithm can be summarized into three items: reckon of top-of-atmosphere radiance of the image, cloud detection using an SVM classifier, and finally refinement of results. The three stages are described separately in the following.

The top-of-atmosphere radiance of the image is computed using the absolute calibration factor. The formula used in this process is:

$$B_i = \frac{p_i X}{E_i * \sin\theta_s}$$

Where 'p_i' stands for the spectral reflectance for spectral band '*i*', 'X' for the pixel radiometric count, 'E_i' for the mean spectral irradiance in spectral band '*i*', and 'θ_s' for the solar elevation angle. The same formula can be also defined as:

$$p_i = \frac{\alpha i}{\cos\theta_s}$$

$$B_i = CNB * p_i$$

$$X = \{B_i\}$$

Where 'p_i' is the radiometric calibration coefficient, and 'αi' is a calibration constant, whose value depends on the considered spectral band *i*. 'CNB' represents the uncorrected data.

The second phase, i.e. the SVM classification, consists of applying a scalar product between '$x_{\{l,p\}}$' and the SVM weights. The classification action of the algorithm is simply defined as:

$$\langle \vec{w} \cdot \vec{x}_{l,p} \rangle + b \begin{cases} \geq S, & Cloudy\ pixel \\ < S, & Cloud - free\ pixel \end{cases}$$

Where 'w' represents the weights of the SVM. In addition, two SVM parameters must also be considered, which are defined as 'b' and 'S'. The first one is a bias value, and the second one is the threshold applied to identify cloudy pixel. The cloud detection is a binary problem, and in a binary classification the two parameters could in principle collapse into one; still, in our case we keep them separated to avoid changing an established convention.

The last phase is the refining of the classification results. It is done by applying a mask to eliminate isolated pixel (i.e. with no neighbors) classified as cloudy. It was noticed that this process reduces the false positive rate in cloud detection. The mask can be applied using either a *city block* (4- neighbors) or a *chessboard* (8- neighbors) distance.

The computational costs are described in section 6.1.1. The bit-depths of the algorithm parameters are available in Table 1, and they are defined by the (Camarero, Thiebaut, Dejean, & Speciel, 2010).

Pixel Value	16 bits
αi	14 bits
$1/\cos\theta_s$	16 bits
W	16 bits
b	16 bits
S	16 bits

Table 1: Bit-depth of the cloud detection algorithm

In case of the Sentinel-2 satellite, the first processing levels (i.e. 0, 1-A, and 1-B) are sub-images of a given number of lines along-track and separated by detector. They are 25 km across track and 23 km along-track in size. Sentinel-2 completes a single orbit in 100 minutes and during each orbit it acquires approximately 3500 images. This means that each image is acquired in around 1.7 seconds. Moreover, the number of bands equals to 13, and they are clustered in different spatial resolutions which are: four at 10m, six at 20m, and three at 60m.

The cloud detection algorithm for Sentinel-2 data is reckoned using 3 bands, resampled at 60m spatial resolution. Detection is carried out mainly applying thresholds, and constraints, over spectral reflectance pixel values. The pixel size of the image at 60m equals 416 x 383.

3.3 On-board compression

As already cited in D1.1, many data compression techniques have been proposed during the last few years. Nowadays, anyway, the attention is focused on algorithms that can be compliant with the on-board available resources both in term of memory usage and in term of computational performances (or capabilities). Only this latter impact is considered in this evaluation step and "measured" for homogeneity in FLOPs as defined in the Introduction.

Recently, the CCSDS has defined a standard for efficient compression of multi/hyperspectral data, that, for the required computational capabilities, can be implemented with the on-board available resources. The CCSDS 123 compressor is then the coding standard suggested for on-board pre-processing, lossless compression (as already mentioned in D1.1).

In order to analyze the impact of the CCSDS 123 algorithms on performance requirements, we have decided to refer to (Santos, Berrojo, Moreno, J., & López, 2016) as a most relevant example of recent

and feasible on-board implementation. The authors have synthesized, in fact, such a system on space-class FPGA Microsemi RTAX1000S (other authors, e.g. (Lopez, Napoli, & Strollo, 2015), developed a version of compression algorithm specific to another space-class FPGA, branded Xilinx).

Since the algorithm is almost hardware-linked, and its performances are related to many input parameters, some practical hypotheses have to be done in order to reach to the end of the actual FLOPs requirements computation. This avoids the, meaningless, performances analysis in all available combinations of input parameters.

From a computational point of view, the algorithm can be split into two main steps:

a) **Prediction Phase**: this part of the algorithm consists of the prediction of a current pixel based on some sort of correlation with the previously visited pixels. The "previously visited pixels" can be just the previous spectral band pixels (*reduced prediction*) or, in addition to these latter, also 4 spatially neighboring pixels (*full prediction*). After this prediction, a residual is obtained for all image samples and then is stored in a matrix in order to obtain the so-called "Mapped Prediction Residual".
b) **Encoding Phase**: The mapped prediction residual is then suitably coded by means, for example, of an entropy coder.

Parameter	Range	Default value selected for FLOPS computation	Description
Number of band for prediction (P)	[0-15]	P (3 typical; 15 in the "worst" case)	Number of "nearby" bands used to perform the prediction.
Prediction mode	Full/reduced	Full	Indicates whether the directional local differences are used in the prediction (i.e. if spatial info. are used to perform the prediction).
Local sum mode	Neighbour/Column	Neighbour	Define the neighborhood used to compute the local sum.

Table 2: Main input parameters of compression algorithm

Form a computational standpoint, the computational constraints can be extracted by just analyzing the Prediction Phase, being this latter the most demanding one. The encoding phase, indeed, can be in principle considered to be implemented by a *look-up-table*, which does not impact on the FLOPs computation. This latter block only impacts on the memory requirements, both in terms of the number of cells but also in terms of access time. **We thus assume that the performances of the algorithm are characterized by the Prediction step only**, which is detailed in section 6.1.2.

The input parameters of the prediction phase are different, but just a few actually affect the performance of the algorithm in terms of FLOPs. The significant ones are listed in Table 2.

3.4 On-board band registration

Nowadays, automatic band-to-band registration of multispectral images is routinely performed on-board satellites (Yu, Vladimirova, & Sweeting, Autonomous band registration for on-board applications, 2007, November). Performances depend on the robustness and accuracy of band registration algorithm. In this project, a specific algorithm was selected for on-board implementation after a deep analysis of the state-of-art in scientific literature. Such algorithm is described in (Yu, Vladimirova, & Sweeting, Autonomous band registration for on-board applications, 2007, November) and proposes an automated band-to-band registration system, which uses a new gradient-based phase correlation method with an added sub-pixel extension stage.

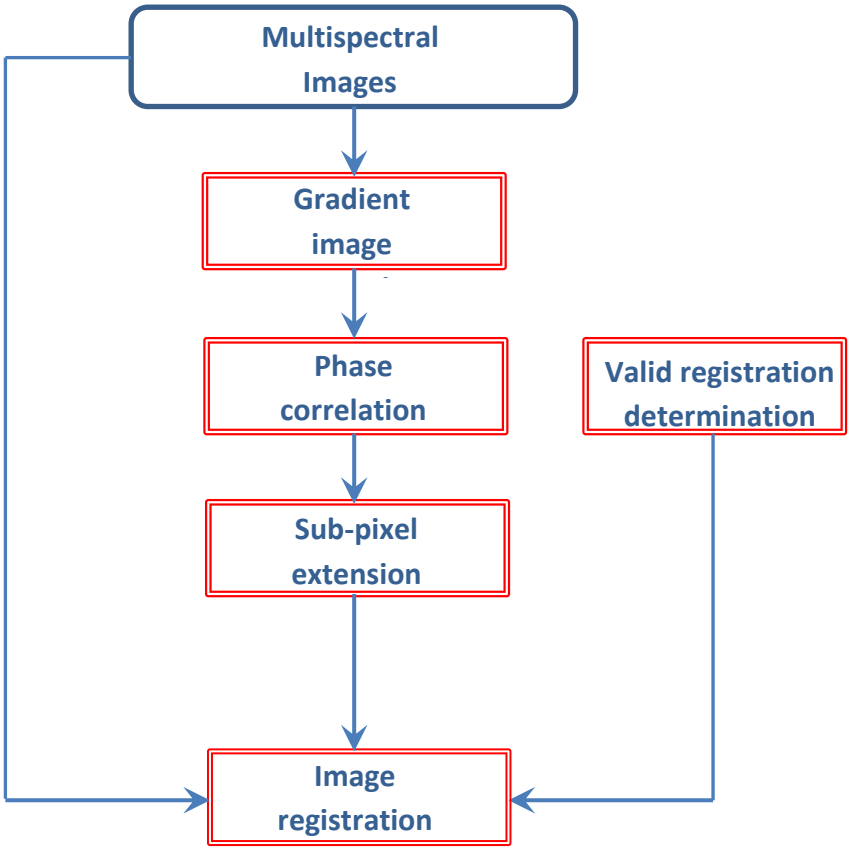

Figure 1: general workflow of the band-to-band registration methodology

As shown in the workflow depicted in the Figure 1, the proposed registration system consists of four stages: gradient image generation, phase correlation, sub-pixel extension, and valid registration determination.

The first stage foresees the computation of the local absolute gradient over the entire image for each single band composing the dataset. This is done because the local absolute gradient is assumed to be highly correlated across the various spectral bands, due to e.g. object edges causing same-place transitions at all wavelengths.

For the second step, two bands are considered at a time, one being the unique reference one onto which all the others are registered. The gradient-image based phase correlation still fails in some

homogenous areas, which contain mostly noise without any useful features. The system must also be able to detect cases when it fails, which is the aim of the autonomous registration process.

Two criteria must be met, before registration can be deemed successful. If not, a failure is detected and an alert issued.

The first criterion relies on the identification of images that are too noisy for the alignment strategy to operate correctly. The correlation function is tested for distance between the highest and the second highest peak:

O. 625 ·Peak 1 > Peak 2

where Peak 1 is the overall maximal peak of the phase correlation; Peak 2 is the second maximum peak. If the above inequality does not hold, then the probability that the overall maximal peak is a valid indication of the band displacement can be considered too small.

In this case "distance" is computed as Euclidean distance:

$$\mathrm{D}: \sqrt{x^2 + y^2}$$

The second criterion is as follows:

Sum1 >Sum2 and Sum1 >Sum4

where Sum1 is the sum of the values of all points the distance of which to the maximal peak (Peak 1) is 1. It is computed by summing values of all pixels whose distance to the peak is 1 or less. Similar definitions apply for Sum2 and Sum4. When the input images are not very noisy, the correlation around the main peak normally degrades sharply; if any of the above two conditions is not met, then the image is probably too noisy to lead to successful co-registration.

SUB-PIXEL REGISTRATION

After correlation computation, the correlation peaks are analyzed to determine the amount of sub-pixel displacement. Assuming the maximal peak is at (x_p, y_p), and the two closest secondary peaks are at (x,y_p), and ($x_{p,y}$) with x_s=x_p ±1 and y_s=y_p ±1, two solutions are given below:

$$\Delta x = \frac{PC(x_{s,}y_p) * x_s + PC(x_{p,}y_p) * x_p}{PC(x_{s,}y_p) + PC(x_{p,}y_p)}$$

$$\Delta x = \frac{PC(x_{s,}y_p) * x_s - PC(x_{p,}y_p) * x_p}{PC(x_{s,}y_p) - PC(x_{p,}y_p)}$$

Only one of the Δx values given by the two equations is valid and it must lie between x_s, and x_p. The method does not need an interpolation. The same approach is used to determine Δy:

$$\Delta y = \frac{PC(x_p,y_s) * y_s + PC(x_p,y_p) * y_p}{PC(x_p,y_s) + PC(x_p,y_p)}$$

$$\Delta y = \frac{PC(x_p,y_s) * y_s - PC(x_p,y_p) * y_p}{PC(x_p,y_s) - PC(x_p,y_p)}$$

IMAGE REGISTRATION

Finally, registering the (b-1) bands to the b-th one implies shifting each pixel by the amounts Δx and Δx.

Assuming a non-integer shift, which implies interpolation, the used formula is:

New_value(x): $X_i + (X_{i+1} - X_i) \cdot \Delta x$

New_value(y): $Y_i + (Y_{i+1} - Y_i) \cdot \Delta y$

3.5 Mission Concept and Design

The selected optical Use Cases can be divided into two macro-categories. One regards the panchromatic applications, which include Ship Detection & Type Identification and Homeland Security, that have a resolution requirement of less than 1 meter with a swath of usually 50 km, while the other regards a Multispectral (Visible + SWIR + NIR) mission (namely the Oil Spill Monitoring), which has a larger swath (>100 km) in a 1000x1000 km area and a slightly lower resolution (1-10 m). These two categories can be addressed by several approaches: as a guideline, two are here presented.

3.5.1 Patchwork

The first approach, useful for the first category, combines the need of small platforms (with consequently smaller optics) with the necessity of higher resolutions, without neglecting the swath size. Using a formation of multiple satellites in lower orbits, it is possible to achieve the required performances combining the images collected by the cluster. Overlapping the acquired images, the final acquisition can be hence reconstructed. This approach requires a precise pointing accuracy and attitude knowledge, in order to accurately combine the acquired images. This “patchwork” approach isn’t always feasible nor easy to implement, thus it shows the greatest effectiveness when it is used to cover areas limited in time and space.

The following example shows a plausible set of parameters for a Ship Type Identification mission, consequent to a previous Ship Detection mission that identified potential areas of interest.

This application requires a spatial resolution less than **5 meters**, with a swath width of **50 km** in panchromatic bands. To address this scenario, a cluster of small satellites is proposed, in order to provide the adequate coverage (which is set to **50x50 km**, according to the proposed User Needs).

Using a cluster of three small satellites orbiting at **550 km**, with a TDI factor of **8x** provided with a pitching/rolling manoeuver, the first critical design parameter becomes the off-nadir ground resolution, which must be less than **5 m**, from **37 degrees** off-nadir angle. This angle can be acquired

with both attitude manoeuver and instrument orientation. In addition to this, another important parameter is the minimum slew rate necessary to maintain the correct TDI factor. This is calculated to be at least **0.65 degrees/second** along the track.

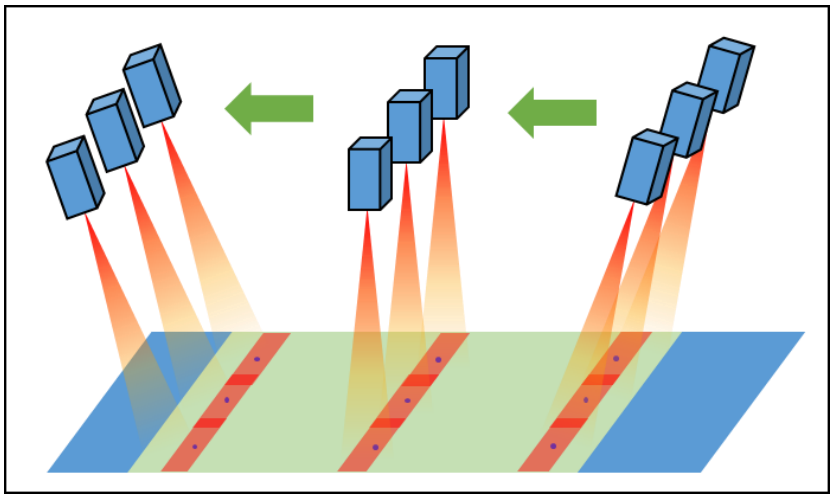

Figure 2: Patchwork swath overlapping in Optical EO

In order to have a **10%** of ground overlay between the three platforms' images, the relative position between the three satellites must be known with a precision of less than **5 meters** and their pointing accuracy must be **150 arcsec** or better, with an error knowledge of **50 arcsec** or better. For observation purposes, the pointing stability of each platform of this cluster, then, must be **30 arcsec/s** or better.

Using a small platform, with a telescope focal length of approximatively 1200 mm, an 1x8000, 7 μm pixel (cross-track) CCD panchromatic array sensor is sufficient to provide the required FOV. Since the ground speed of the track (considering the tilting maneouver) is **873 m/s**, the pixel line is subject to an exposure time of **3.6 ms** for each ground pixel strip with the desired GSD. The sensor pixel line is then integrated (in this approximation, read-out time is considered negligible, since it takes a very small fraction of the overall integration time, in the order of μs). Considering 10 bit per pixel depth, each 3.6 ms a strip of 1x8000 pixels is acquired with 10 bits per pixel. Therefore, every 3.6 ms (272 Hz) , 80000 bits are generated, leading to a data throughput of **~21 Mbps**.

The reconstruction of the full image needs the three acquisition to be characterized in terms of time precision. Since the sampling frequency is about 272 Hz (1x8000 pixels every 3.6 ms), the relative time precision and time synchronization between the platforms should be at least in the order of magnitude of **1 ms**. The timing knowledge of the overall cluster, instead, could be relaxed to three orders of magnitude higher (namely **1 s**), leading to a reasonable 2% coverage error on the area of interest.

Table 3: Patchwork case, communication summary table

Requirement Type	Data Amount	Available Time	Data Rate Limitation
Uplink	no specific requirement	600 sec (average)	64 kbps TC 2 Mbps TM (low consumption S-band TM downlink)
Downlink	1.16 Gb/acquisition/sat.	600 sec (average)	300 Mbps (X-band downlink)
Inter-Satellite-Link (ISL)	n/a	n/a	n/a

3.5.2 Spectrum fractionation

In the second case, the fractionation does not regard the size of the image but rather the spectral bands. In this case, the platforms fly in a close formation one after the other on the same path, each acquiring a different set of spectral bands (VIS, SWIR, NIR). These images need to be correlated and overlapped in a very precise way, so the position knowledge for each of the platform must be as precise as the smallest pixel dimension. Given the fact that the Oil Spill Monitoring requires a resolution of at least **1 m**, the relative position of each platform is required to be known with at least this precision.

Also, the time of each acquisition must be known within an error that is of the **same magnitude of the quickest event** the system wants to observe. In the considered application, the quickest event would probably be the swell of the seawater, so the order of magnitude would be **1 second**. This means that the time error between each acquisition of each satellite must be of this order of magnitude.

This leads also to the definition of the relative position among the systems: given a specific orbit, the time that elapses between the acquisitions must be of the same magnitude. In a LEO formation, this distance can be few kilometers while in higher orbits this values drops to a few hundreds of meters.

Table 4: Spectrum fractionation, communication summary table

Requirement Type	Data Amount	Available Time	Data Rate Limitation
Uplink	no specific requirement	1000 sec (average – 800 km of altitude)	64 kbps TC 2 Mbps TM (low consumption S-band TM downlink)
Downlink	40 Gb/orbit/sat, 500 Gb full AoI	1000 sec (average – 800 km of altitude)	250 Mbps (X-band downlink)
Inter-Satellite-Link (ISL)	n/a	n/a	n/a

The above two cases of formations of multiple satellites do not assume autonomous formation flying and also no share of payload data between the satellites. However, if the formation is supposed to be autonomous, a low data rate ISL link is required.

4 SELECTED RADAR USE CASES

This section analyses in further detail the pre-selected radar use cases from the requirement collection document D1.1. In particular the following two use cases are further discussed:

- *Resampling and decimation of data for a Staggered SAR system*
- *Generation of focused, high resolution (bistatic/generic) SAR images*

In addition the requirements on the following enabling methods and technologies are quantified:

- *Synchronisation of time and phase for bistatic data*
- *Multi-looking of focused SAR images for efficient downlink in support of near-real time applications*

4.1 Resampling and Decimation of Staggered SAR data

As discussed in D1.1, staggered SAR is an innovative concept to support High Resolution Wide Swath (HRWS) radar imaging. It is based on multiple elevation beams and makes use of a continuous variation of the pulse repetition interval (PRI) in order to avoid blind ranges associated with the transmit events of the sensor, during which the receiver must be switched off (Villano, Krieger, & Moreira, 2014.) The price to be paid is a decrease of the average pulse repetition interval, which is required for proper resampling of the data prior to processing. In order to avoid the associated increase of data volume for downlink, it is proposed to implement the resampling and decimation filter on-board the satellite.

4.1.1 Radar Mission Requirements

An example of upcoming polarimetric and interferometric spaceborne SAR mission, which uses staggered SAR for some of its operation modes, is Tandem-L, whose aim is monitoring dynamic processes on the Earth's surface with unprecedented accuracy and resolution.

The amount of data acquired within one data take is strongly dependent on the acquisition mode. For the main single-pol acquisition mode, where staggered SAR is used to map a 350 km continuous ground swath, assuming a 200 km length for the data take, a range sampling frequency 10% higher than the 84 MHz chirp bandwidth and a mean PRF on transmit of 2600 Hz, the number of range and azimuth lines are equal to 69 517 and 130 907, respectively, leading to a total number of 9.1 billion complex samples.

As described in (Villano, Krieger, & Moreira, 2014.), the optimization of the sequence of PRIs to be employed leads to the selection of a "more elaborate" sequence of PRIs, which is in this example, consists of a sequence of 225 distinct PRIs, which then repeat periodically for the full duration of the acquisition (Figure 3).

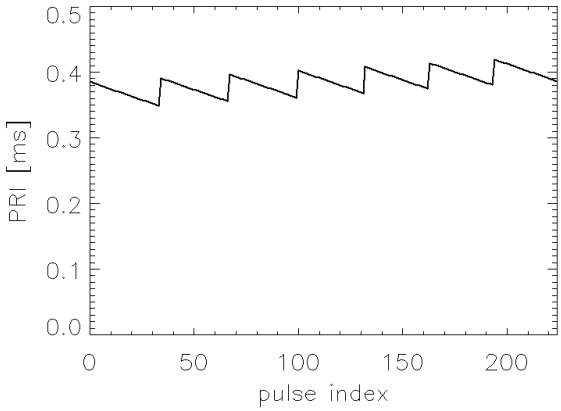

Figure 3: Sample sequence of PRIs to be used for the single-pol acquisition mode. The mean PRF on transmit is 2600 Hz.

The proposed method for data volume reduction will significantly reduce the amount of samples of each azimuth line. After each azimuth line is resampled, Doppler filtered and decimated (see also 4.1.1.1 for a top level description of the algorithm), the azimuth sampling frequency of the data to be downlinked will be equal to 1.2 times the processed Doppler bandwidth (PBW), i.e. 1352 Hz, for PBW = 1127 Hz. The number of range lines of the considered sample data will become 36 159, while the number of azimuth lines will remain the same. The volume of data volume will be therefore reduced by almost 48% with an absolutely negligible degradation of the image quality. Figure 4 shows the effect of the discussed data volume reduction strategy on the 2-D impulse response function (IRF). The slight degradation of the AASR (smaller than -55 dB) occurs due to the localized azimuth ambiguities.

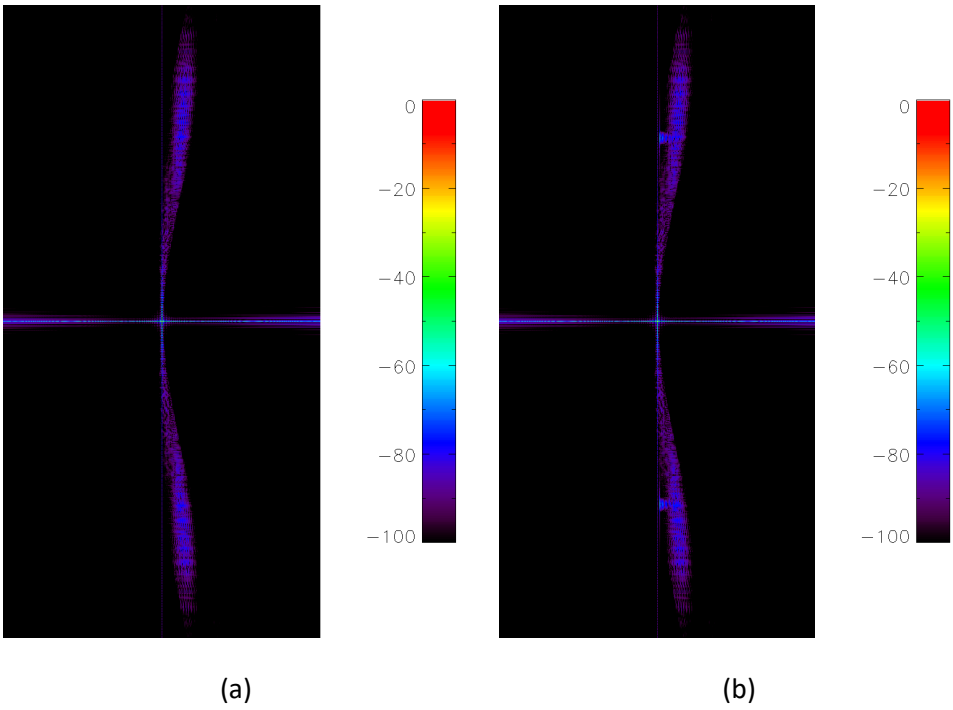

Figure 4: Effect of data volume reduction on the 2-D IRF for a staggered SAR. The horizontal and vertical axes represent slant range and azimuth, respectively. The size (slant range × azimuth) is 1.7 km × 40.6 km. (a) 2-D IRF in dB, in case all data are downlinked. (b) 2-D IRF in dB, in case data are decimated by a factor of 3, after having filtered them with a 25-tap Wiener filter. The additional localized azimuth ambiguities due to decimation are visible.

4.1.1.1 Top Level Algorithm Description

The filter to be implemented for the resampling and decimation of staggered SAR data is a combination of a Best Linear Unbiased (BLU) estimator and a low-pass filter. Considering that the BLU parameters rely on the coefficients of the autocorrelation functions, it is clear that the knowledge of the antenna size, system PRF and a limited amount of oversampling is required. For efficient SAR operation the amount of oversampling shall be minimized and thus it can be stated that the BLU coefficients will be limited to at most 5. On the other hand, the low-pass filter FIR coefficients are in the order of 20. For efficient implementation, these two coefficients shall be combined prior to applying them to the data, as indicated in Figure 5. In summary Doppler filtering for staggered SAR requires computing and saving the coefficients to weight the input data and performing multiplications and summations to produce the output data. The coefficients are different for each range and azimuth sample, but they repeat in azimuth after a number of samples equal to the number of PRIs of the sequence (in the order of 200-300). It has been estimated that a memory in the order of few Gbit is required for the Tandem-L staggered SAR system.

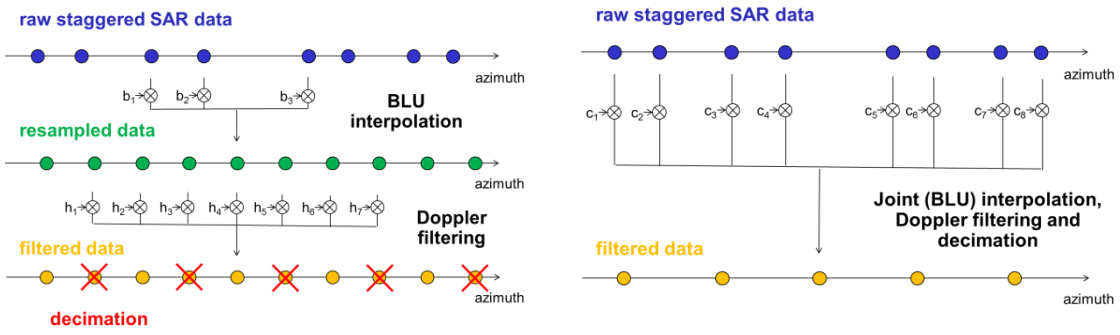

(a) (b)

Figure 5: (a) Interpolation, Doppler filtering, and decimation in the staggered SAR case. (b) Equivalent scheme, where interpolation, Doppler filtering, and decimation are jointly performed.

The top level algorithm is described as follows:

For each output azimuth position:

- *select azimuth positions of input data according to FIR filter length*

for each range position:

- *Compute/load the proper filter coefficients*
- *Compute weighted addition of samples.*

4.1.1.2 Requirements for On-board Processing

It is proposed to precompute the weighting coefficients in advance and store them on-board. The required operations consist in complex data multiplications and additions, ideally performed on vectors of length corresponding to the sequence length of repeating PRI (200-300 samples).

4.1.2 Preliminary Benchmarking Plan

The preliminary benchmarking plan foresees functional tests to validate the proper algorithm implementation and benchmarking tests for estimation of throughput characteristics of the concept compute system and for scaling purposes related to a future on-board compute system.

4.1.2.1 Functional test

The functional test shall operate on a single azimuth line (constant range) of staggered SAR data and shall validate the resampling and decimation step. It must ensure perfect match between the prototype implementation and the target implementation. The required computation time is a first estimate for scaling the block size of the subsequent benchmarking tests, taking into account the dimensioning of the concept compute system available in S3NET. It may operate on a limited vector length corresponding to 3 PRI cycles.

4.1.2.2 Benchmarking tests

Once the functional test is passed, the efficiency of the implementation shall be estimated for a representative 2D data subset. For this purpose, first, the resampling and decimation steps shall be repeated for several thousand range positions, including the proper update of filter coefficients. Second, the operations shall be extended to work on several azimuth blocks.

4.2 Generation of focused, high resolution (bistatic/generic) SAR images

The second radar use case relates to SAR image formation on-board the satellite. Within S3NET the discussion will be limited to traditional stripmap SAR data, thus avoiding the additional algorithmic complexity of wide-swath or high-resolution SAR modes (e.g., ScanSAR, TOPS, Spotlight). However, the benchmarking results to be obtained within S3NET will give a first guess also on the feasibility of on-board processing for these specific modes. In this section the discussion is primarily on requirements for monostatic SAR data processing, whilst the additional complexity imposed by bistatic operation is just indicated, leaving the discussion to section 4.3.

4.2.1 Radar Mission Concept

The preliminary radar mission concept assumes a C-band radar instrument, similar to the one on-board Sentinel-1, operating in stripmap mode, i.e. with a resolution of 5m by 5m and swath width of 80km (Torres, et al., 2012). It is anticipated that such an imaging mode will be supported also by the next generation Sentinel-1 satellites, which were selected as the master Tx satellite for the SESAME formation described in D1.1.

4.2.2 Radar Mission Requirements

This mission concept requires that SAR image formation is performed on board the satellite. This requires the efficient implementation of a precise SAR image formation algorithm for the on-board compute system. For the purposes of S3NET a range migration (also known as w-K) algorithm with modified Stolt mapping is selected because it doesn't make any approximations and is suitable also for squinted SAR operation, a potential requirement for bistatic SAR data (Cumming & Wong, 2005), (Reigber, Alivizatos, Potsis, & Moreira, 2006), (Vandewal , Speck, & Süß, 2007).

4.2.2.1 Top Level Algorithm Description

The functional block diagram of the extended w-K algorithm (EOK), as first proposed in (Reigber, Alivizatos, Potsis, & Moreira, 2006) is presented in Figure 6, however, omitting the motion

compensation steps, which are (mostly) irrelevant for spaceborne surveys. As indicated in the diagram, the algorithm consists of Fast Fourier transforms (FFTs, in blue), complex data vector/matrix multiplications (range compression, azimuth compression, wave migration, in green) and 1D interpolations (modified Stolt Mapping, in orange).

In addition, the diagram includes data pre- and post-processing blocks. Some sensor-specific pre-processing options were described in D1.1 and can be:

- Digital beamforming in elevation according to the Scan-on-Receive (SCORE) concept;
- Multiple azimuth displaced phase centre signal recombination (MAPS);
- Synchronisation of time and phase for bistatic data (see also section 4.3)

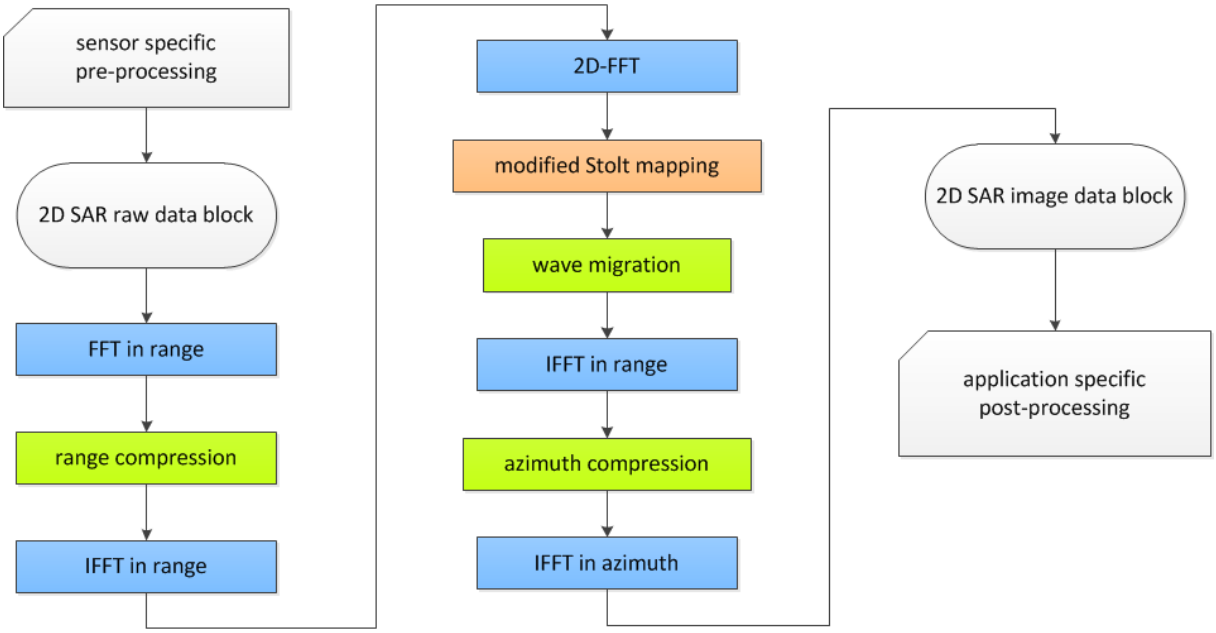

Figure 6: Functional block diagram of the EOK algorithm

Also application specific post-processing blocks were described in D1.1.

- Multi-looking of focused SAR images (see also section 4.4)
- Level-2 product generation for maritime/oceanographic applications
- Region-of-Interest (ROI) defined full resolution mapping for land applications
- On-board interferogram computation for single-pass interferometric SAR (e.g., VERITAS, SESAME)

These are relevant especially for reducing the data amount for downlink.

4.2.2.2 Requirements for On-board Processing

Considering the selected C-band radar mission concept, the EOK algorithm for on-board SAR image formation requires operations on complex valued data vectors/matrices of size 23000 by 34000, corresponding to one SAR image covering 80km by 120km with state-of-the-art resolution of 5m. However, if these dimensions turn out to exceed the memory of the S3NET concept compute system or the ones of a future on-board processing system, overlapped block processing can be applied. In this case a first compromise between computational efficiency and required on-board resources

would suggest blocks (complex float data matrices) in the order of 16384 x 16384 complex samples. This would correspond to an on-board RAM requirement of at least 2x 2GByte (factor of 2 to allow intermediate storage after each operation).

In addition to these requirements, it should be mentioned that the input data rate from the ADCs is in the order of 100 Mbyte/sec, consisting of byte formatted SAR raw data, which need to be converted to complex float prior to processing.

4.2.3 Preliminary Benchmarking Plan

The preliminary benchmarking plan foresees functional tests to validate the proper algorithm implementation and benchmarking tests for estimation of the throughput characteristics of the S3NET concept compute system and for scaling purposes related to a future on-board compute system.

4.2.3.1 Functional tests

The functional tests shall operate on a 2D block of raw data. A dedicated test has to be foreseen for each step of the algorithm. These tests must ensure perfect match between the prototype implementation and the target implementation. The required computation time for each test is a first estimate for the overall computation time to be expected for the implementation on the S3NET concept compute system.

4.2.3.2 Benchmarking tests

Once the functional tests are passed, the efficiency of the implementation shall be estimated for one 2D raw data block considering all algorithm steps. This shall allow upscaling for the case of processing one complete scene.

4.3 Synchronisation of time and phase for bistatic data

4.3.1 Radar Mission Concept

The preliminary radar mission concept assumes the same Sentineel-1 like C-band radar illuminator (referred to as the master or chief) as discussed in section 4.2.1 and at least one receiver on a companion satellite flying in a bistatic formation (SAOCOM-CS & SESAME formation concepts described in D1.1.) (referred to as slaves or deputies). The motivation is adding single-pass interferometric capabilities to the master/chief satellites imaging performance. Interferometric combinations of master and slave (chief and deputy) allow inferring the third dimension which provides information, e.g. on forest height and structure and/or ice sheet topography. If the companion(s) are displaced in along-track, information on moving targets and ocean currents can be extracted.

4.3.2 Radar Mission Requirements

The radar mission concept requires the bistatic SAR data recorded by the companion receive satellites to be synchronized to the master satellite, to compensate the relative clock frequency offsets and different timing references of the systems, thus ensuring the proper recording of the reflections from the illuminated swath and recoverable relative phase offsets. Otherwise, the consequences may be of severe impact, ranging from a significant increase in the data rate to intolerable phase and timing errors which may lead to the impossibility of interferometric processing, significant geolocation errors, and strong defocussing.

For SAOCOM-CS the master and companion satellite are non-cooperative, i.e. they do not exchange information during the data acquisition. Clock synchronisation is effected at ground segment level following a two-step approach: a) firstly, a coarse estimate of time and frequency offsets is computed by averaging the GPS time references of transmitter and receiver compared to the instrument times, and b) a fine estimation step based on an autonomous synchronisation (i.e., AutoSync) approach (Rodriguez-Cassola, et al., 2012). The AutoSync approach requires the joint evaluation of the focussed monostatic and bistatic data, which, if performed on-board, would impose enormous demands on the inter-satellite link and on-board computational capabilities. A further solution yielding better overall performance is the use of a direct link between transmitter and receiver, as was done in the TanDEM-X mission. In TanDEM-X, a cooperative bistatic SAR formation, clock synchronisation is achieved after the evaluation of the radar pulses exchanged by transmitter and receiver satellites during the bistatic acquisition (Krieger, et al., 2007), which requires direct visibility between the systems.

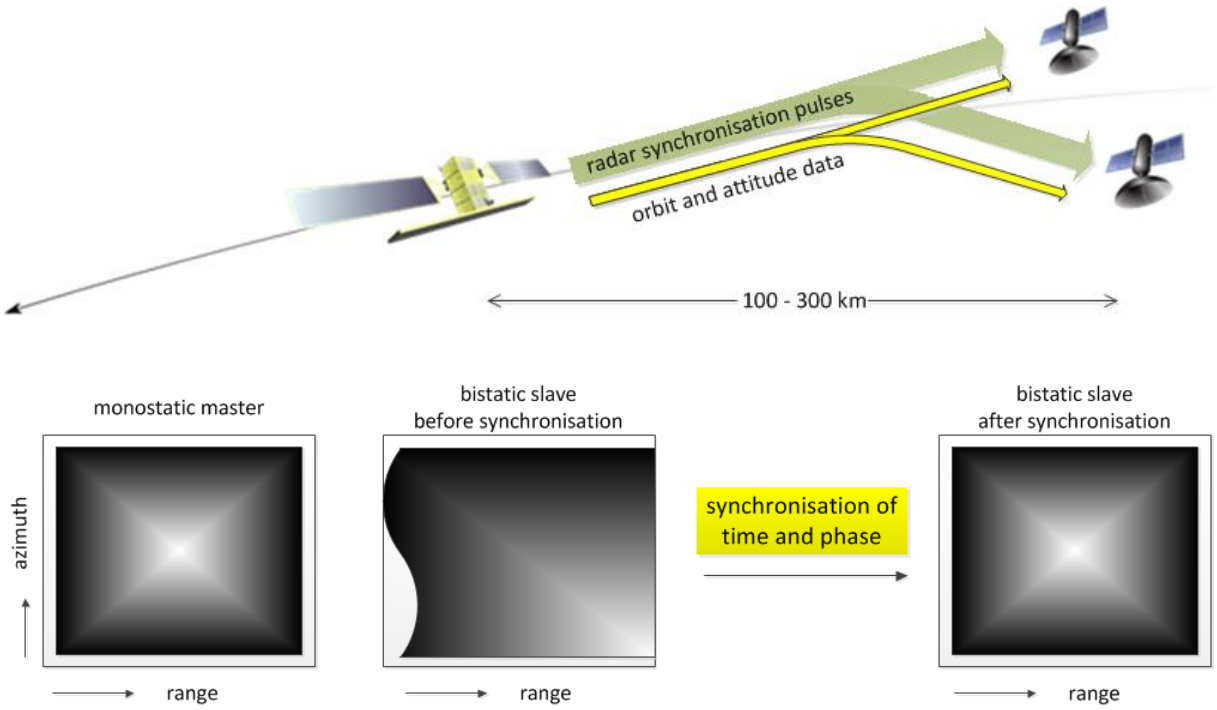

Figure 7: Companion satellites, synchronisation data exchange and compensation of bistatic SAR data

Within S3NET we consider the one-directional exchange of the transmitted chirp from master to slave. It can either be dedicatedly transmitted by the master towards the slave through synchronisation horns at periodic intervals, or it may be received through sidelobes of the transmit and receive antennas each time the master transmits a radar pulse towards ground. In both cases the received direct signal needs to undergo a conditioning to provide the synchronisation parameters for the proper SAR image formation processing. This conditioning requires precise (relative) orbit positions for compensating the varying propagation delays between master and slave.

4.3.2.1 Top Level Algorithm Description

The functional block diagram for the conditioning of the sync signals and the synchronisation processing of the bistatic SAR data is presented in Figure 8. It corresponds to the sensor-specific pre-processing task in the SAR image formation algorithm block diagram in Figure 6.

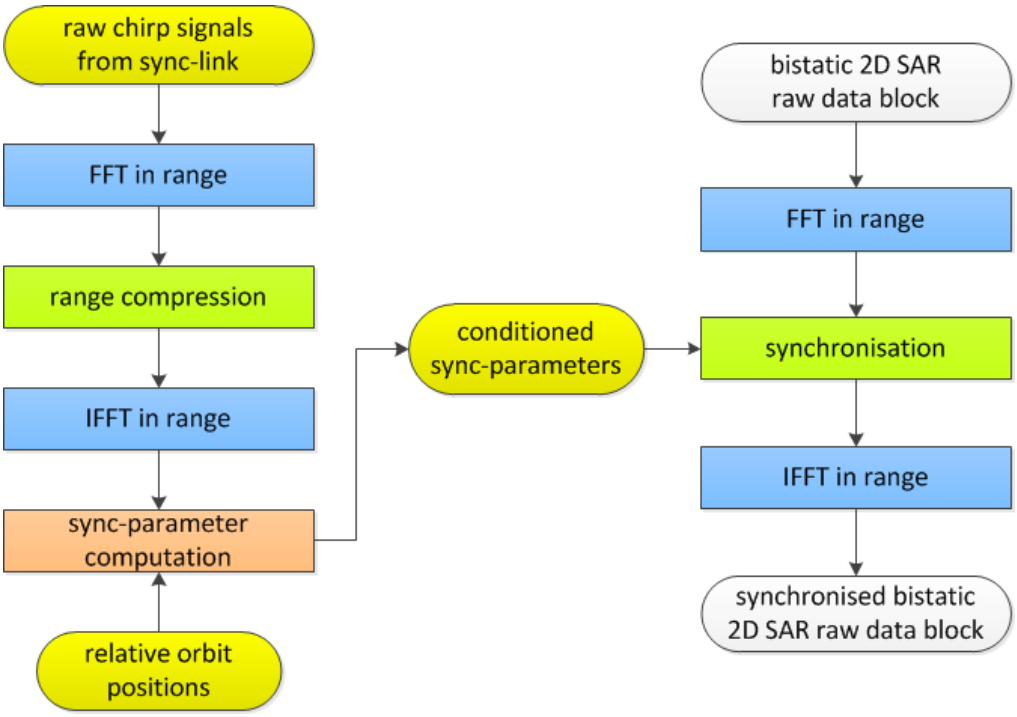

Figure 8: Functional block diagram for the synchronisation of bistatic data.

The synchronisation data (yellow) need to be processed in a first step independently from the SAR bistatic data. This processing is performed on a reduced data amount, since the variation of sync parameters has a low-pass characteristic compared to the SAR data (left side of the block diagram). However, the derived sync parameters need then to be up-sampled to the higher sampling of the bistatic data. This and the alignment of the orbit data require 1D interpolation (orange).

The synchronisation of the bistatic SAR data is performed in a second step (right side of the block diagram). It makes use of FFTs (blue) and complex vector/matrix multiplications (green). The sequence of operations and computational load is similar to the range compression processing task of the SAR image formation radar use case (see Figure 6). Thus these two steps can be joined for efficiency reasons in a final algorithm implementation. It needs to be mentioned that further adaptations to the generic SAR image formation algorithm are required, depending on the formation geometry, which go beyond the synchronisation task described in this radar use case.

4.3.2.2 Requirements for On-board Processing

If the synchronisation processing of the bistatic data is performed jointly with the range compression processing, the requirements for bistatic on-board SAR image formation are only marginally higher than for the monostatic case discussed in section 4.2. Although the additional conditioning of the sync data operates on similar 1D vector length as the recorded SAR data, i.e. in the order of 16384 samples, it updates of the direct link signal are required only about 10-20 times per second in contrast to several thousand vectors per second of the bistatic data recorded by the Rx-only slaves. Thus similar requirements for the dimensioning of the S3NET concept compute system or a future on-board processing system need to be posed as for the monostatic/generic SAR image formation, although bistatic SAR processing requires in general a numerical computation of the SAR processing functions (modified Stolt mapping, wave migration, azimuth compression in Figure 6), which makes it slightly less efficient than the regular monostatic case.

4.3.2.3 Communication requirements

The communication requirements for this radar use case are primarily related to the exchange of precise orbit and attitude data. In particular the position and attitude of the master satellite need to be transmitted to the slave for the evaluation of relative orbit positions (or vice versa).

In addition and depending on the configuration of the on-board processing system, exchange of the digitized radar data may be required:

- Transmission of digitized data of the transmitted chirp, in case processing is performed on the companion satellite. These data shall be used for calibrating the bistatic SAR data. The data rate is approximately 5-10 Mbit/sec (10-20 times per second 16384 complex samples in byte format) considering real-time operation during a data take.
- Transmission of the bistatic data from the companion satellite to the master in case the on-board processing system or down-link capabilities are only available at the master satellite or combined processing is to be performed at the master. In this case the data rate is approximately 800 Mbit/sec considering real-time operation during a data take.
- Transmission of the monostatic (SAR raw or image) data from the master satellite to the companion in case the on-board processing system is only available at the companion satellite, or the master and slave image combination is to be performed at the slave. Also in this case the data rate is approximately 80 (Rodriguez-Cassola, et al., 2012)0 Mbit/sec, again considering real-time operation during a data take.

4.3.2.4 Formation flying requirements

As mentioned above, precise relative orbit positions are required for the conditioning of the synchronisation data. If processing is to be performed on board, this information is to be provided in real-time or with very short latency (e.g., few seconds). It is important to point out that primarily the change (e.g., derivative) of relative orbit position (i.e., baseline) needs to be known with sub-wavelength precision, whereas the relative orbit position itself needs to be known with fractions of a radar resolution cell if only a good alignment and no absolute phase is required. For the C-band system under consideration the numerical requirements are:

- Knowledge of relative change in orbit position: ideally better than 3.5mm within an orbit path of 5km
- Knowledge of relative orbit position: better than 50cm.

The first requirement relates to phase compensation to ensure proper SAR focussing, while the second requirement is supposed to allow perfect alignment of the echo window position and proper coregistration performance in case of subsequent interferometric evaluation. Herby it is assumed that the interferometric phase will be calibrated on ground, once the final precise orbit data becomes available.

4.3.3 Preliminary Benchmarking Plan

The preliminary benchmarking plan foresees functional tests to validate the proper algorithm implementation both with respect to the conditioning of the synchronisation data as well as with respect to the time and phase correction of the bistatic data. Dedicated benchmarking tests for the estimation of the throughput characteristic concerning the radar data are not required, as more severe tests are covered by the SAR image formation use case in section 4.2.3.2. However,

benchmarking tests shall be designed relating to the (near) real-time evaluation of relative orbit positions using formation flying algorithms.

4.3.3.1 Functional tests

Two functional tests need to be foreseen:

- Conditioning of synchronisation data to validate the algorithmic implementation of the left part of the block diagram in Figure 8.
- Time and phase correction of the bistatic SAR data to validate the algorithmic implementation of the right part of the block diagram in Figure 8.

Both functional tests shall operate on representative 2D blocks of raw data.

These tests must ensure perfect match between the prototype implementation and the target implementation.

4.3.3.2 Benchmarking tests

The benchmarking tests relate to the performance of the formation flying algorithms. The design of these tests shall be a task of the S3NET project partner Technion.

4.4 Multi-looking of focused SAR images

This radar use case represents one out of several application-specific post-processing approaches. It intends to supplement the SAR image formation processing described in section 4.2 and Figure 6. It achieves SAR image Speckle reduction at the cost of spatial resolution. Often, these multi-looked SAR images are more useful for image interpretation as the full resolution quicklook data. Due to the reduced resolution the sampling of the images is also reduced, which inherently leads to data volume reduction beyond the amount of the initial SAR raw data. This is not the case for the full resolution complex-valued SAR image data. Therefore multi-looking is considered as one of the mandatory steps for data volume reduction to follow the SAR image formation on-board.

4.4.1.1 Top Level Algorithm Description

The multi-looking consists of the averaging of pixel intensities from a certain neighbourhood. This requires the detection of the complex valued SAR data. The resulting equivalent number of looks depends on the spectral weighting of the complex SAR data and their oversampling factor. The algorithm shall be designed to achieve at least 4 effective look as a trade-off between resolution and Speckle reduction, however, 8-16 looks will give a much better data compression performance (Curlander & McDonough, 1991) (Cumming & Wong, 2005). The resulting SAR intensity images are in float format. For efficiency reasons they can be scaled to 16-bit integer values which is considered to provide sufficient dynamic range or further compressed with standard image compression techniques, e.g, JPEG2000 standard (JPEG 2000, 2016).

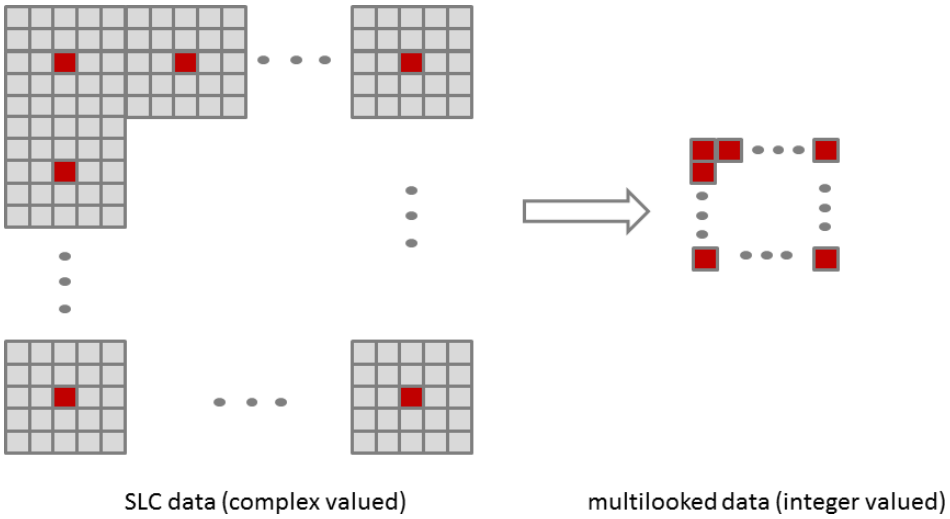

Figure 9: Data volume reduction by means of multilooking. Typical window sizes are indicated for achieving a 16 look SAR image, assuming 20% oversampling of the input SAR image data in both dimensions.

4.4.1.2 Requirements for On-board Processing

The detection of complex valued data requires square operations on matrices. The spatial averaging further requires floating point additions on matrix level (moving average filter). The memory requirements are less than the size of one SLC image data (2 GByte, see section 4.2.2.2), as processing can be performed on subsequent blocks. The amount of floating point operations per output pixel is *3*L*osf*, where *L* is the number of looks and *osf* is the oversampling factor.

4.4.2 Preliminary Benchmarking Plan

The preliminary benchmarking plan foresees a functional test to validate the detection and averaging operations, which can be executed on a SAR image subset. A further benchmarking test shall be designed to evaluate the execution time for a complete SAR image.

4.5 Summary of Communication Requirements for the different Use Cases

The radar use cases are grouped into 2 cases, which are described in the following.

4.5.1 Staggered SAR (Radar Use Case 1)

The first use case relates to the Tandem-L mission concept. In this case the Ka-band technology is limiting quantitatively the overall data acquisition performance.

Table 5: Staggered SAR, communication requirements summary table

Requirement Type	Data Amount	Available Time	Data Rate Limitation
Uplink	no specific requirement	10 min	64 kbps Telecommand; 128 kpbs/2 Mbps Telemetry (programmable) (see (Torres, et al., 2012))
Downlink (no on-board processing, not feasible)	>100 TB/day	10 min	2 x 260 Mbps (X-band downlink; see (Torres, et al., 2012))
Downlink (after on-board processing, Baseline for Tandem-L)	64 Tbit/day	1 day	64 Tbit/day (from 2 satellites, using Ka-band downlink to six ground stations); corresponds to 370 Mbps for one satellite in case of continuous transmit. see (Bachmann, Borla Tridon, De Zan, Zink, & Krieger, 2016)
Inter-Satellite-Link (ISL)	n/a	n/a	n/a

Remarks:

The data rate limitations for the uplink were taken from ESA's S-1 specification, which are considered to be relevant for all radar use cases.

The available time for uplink/downlink corresponds to average visibility of a satellite. From the experience of the German ground station in Neustrelitz with S-1, a typical LOS time in the order of 10 min is realistic.

For the anticipated Tandem-L mission, the data rate limitation of the Ka-band downlink is the major limiting factor for the amount of data to be recorded daily on a routine basis.

4.5.2 Radar formation flying mission (Radar Use Case 2 , 3 and 4)

The second group of use cases relates to the formation flying mission as a potential add-on to the next generation of Sentinel-1 satellites.

Table 6: Radar formation flying, communication requirements summary table

Requirement Type	Data Amount	Available Time	Data Rate Requirement
Uplink	85 MByte (for DEM tiles of 30m resolution covering 200km x 200km)	10 min	1.2 Mbps

Requirement Type	Data Amount	Available Time	Data Rate Requirement
Downlink (no on-board processing)	2x 65 GByte	10 min	2x 86 Mbps
Downlink (after on-board processing, i.e. image generation and multi-looking)	2x 27 GByte	10 min	2x 35 Mbps
Inter-Satellite-Link (ISL) (as an alternative to the downlink)	1.5 GByte / data take 4.8 GByte / data take	17 sec / data take	Requirement: 700 Mbit/sec 2.1 Gbit/sec

Remarks:

For the downlink we consider operation of the formation for a duration of 25 minutes per orbit (S-1 specification in (Torres, et al., 2012) and the availability/visibility of a ground station for each orbit.

The 25 minutes correspond to roughly 90 data takes. In case of no on-board processing the data need to be downlinked by each satellite of the formation (factor of 2). In case of on-board processing, one image and the interferometric phase are downlinked (also a factor of 2, but applies only to one satellite).

5 CLUSTER FLIGHT FORMATION CONCEPTS

The concept presented in section 4.3 imposes strict constraints on the cluster flight. This concept requires a cluster of chief and two deputies. The distance between the chief and the deputies should be a few hundred kilometres, and the distance between the two deputies should be a few hundred meters. The difference between these requirements creates two different cluster flight challenges that need to be solved. We recall previous cluster flight missions and use this knowledge as the foundation of this work.

5.1.1 TanDEM-X Cluster Flight Algorithm Analysis

The TanDEM-X primary objective was to generate high accuracy global digital elevation model using a formation of synthetic aperture radar satellites. Due to similarity between the TanDEM-X and the S3NET requirements, we would like to investigate the control method used by the TanDEM-X mission (D'Amico S. a., 2006) and check if it can be used as one of the alternative for the S3NET cluster flight algorithm.

To define the deputy position with respect to the chief we will use the following triad (see Figure 10) : unit vector $\hat{e}_R$ along the radial direction (positive outwards), $\hat{e}_T$ in along-track (tangential) direction of the satellite motion, and the unit vector $\hat{e}_N$ normal to the orbital plane in direction to the positive angular momentum vector (cross track).

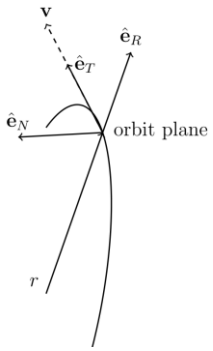

Figure 10: Relative motion orbital frame

The TanDEM-X control concept was to keep the satellite separate mostly by the radial and cross track components. The assumption is that along-track separation is much harder to predict and therefore we cannot rely on this separation to avoid collisions. By keeping the eccentricity and inclination vectors parallel we reduce the risk of collision and keep the cross-track and radial components within bounds. When using near-circular orbits the "regular" orbital elements suffer from mathematical singularities. This approach uses a different set of orbital elements that avoids singularities in near-circular orbits (D'Amico S. , 2010).

To test the control performance we used a high fidelity simulation based on FreeFlyer1 software. We used the TerraSAR-X (TSX) and TanDEM-X (TDX) parameters (Moreira, 2004) as the simulation case

[1] https://ai-solutions.com/

study. TSX main parameters are: mass of 1240 kg, the cross-sectional area is 3.2 m2 and orbit height of 500 km. The TDX has similar parameters, but the initial orbit is slightly shifted to create the required formation. The goal is to keep cross-track separation of 1000 m and radial separation of 300 m. First, we examine the behaviour of the couple without control. Figure 11 (left) shows the changes in the radial cross-track plane in 5 days intervals. We see that by day 25 the ellipse changes to a straight line, meaning high risk of collision. Figure 11 (right) shows the eccentricity vector drift where the blue dot marks day 0 and orange dot marks day 25. At day 0 the x component is nearly zero, and the eccentricity vector is parallel to the inclination vector. Over 25 days the eccentricity vector moves in a circular motion and by day 25 the y component becomes zero, and the eccentricity vector is normal to the inclination vector. It is clear that cluster control is crucial to avoid collision in the cluster.

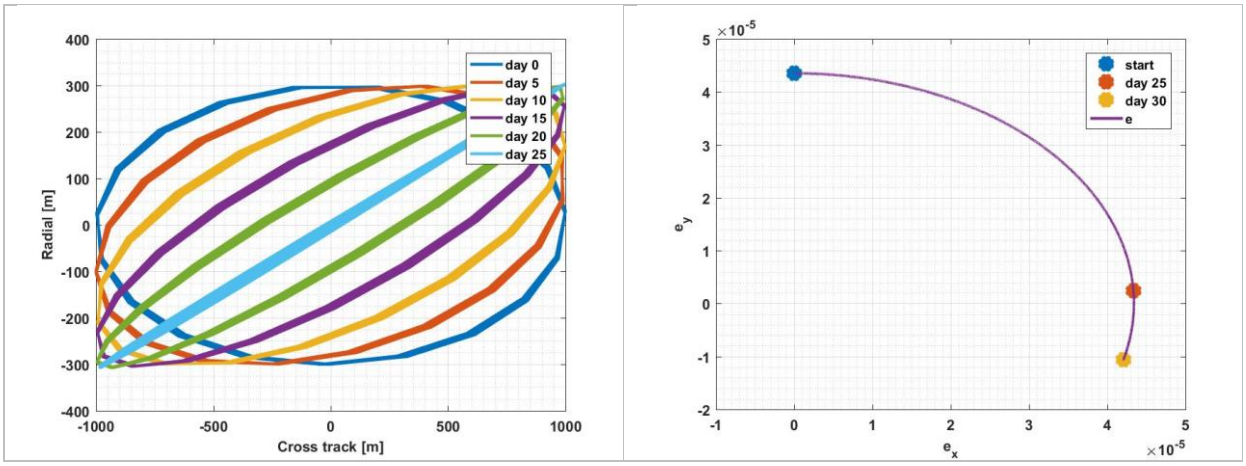

Figure 11: Natural drift of TSX and TDX over 30 days of simulation

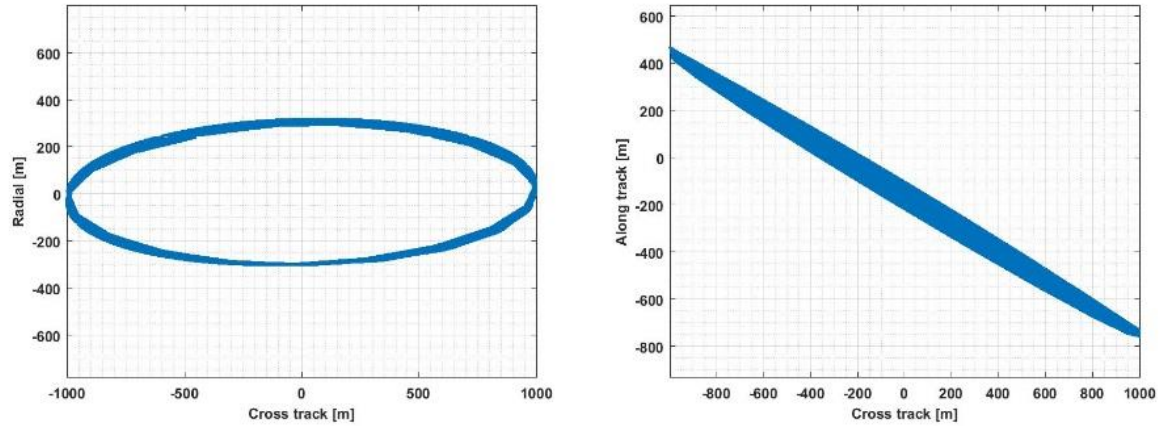

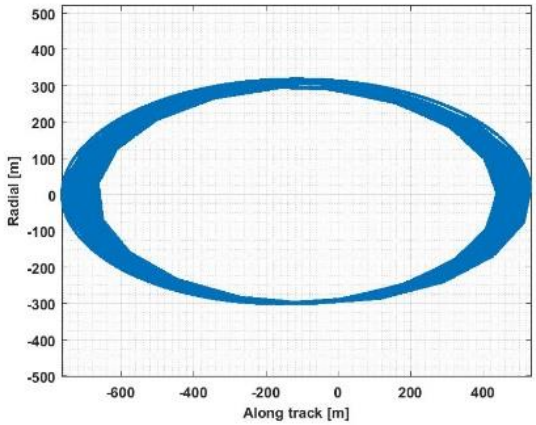

Figure 12: View of the controlled formation from 3 different planes

To reduce the risk of collision and keep the cross-track, along-track and radial components within bounds, we use along-track manoeuvres. Figure 12 shows the controlled cluster behaviour in 3 planes. We see that the cross-track and radial components are kept within bounds. Figure 13 shows the time and magnitude of the required manoeuvres, where each manoeuver was composed of two symmetrical manoeuvres performed by TDX. The manoeuvres were executed near the nodes and the exact position was calculated on-board. The manoeuvres were applied every two days on average. Another possibility would be cross-track manoeuvers that change the cluster baseline. These manoeuvres are useful for SAR and optical missions but can be very costly in term of ΔV.

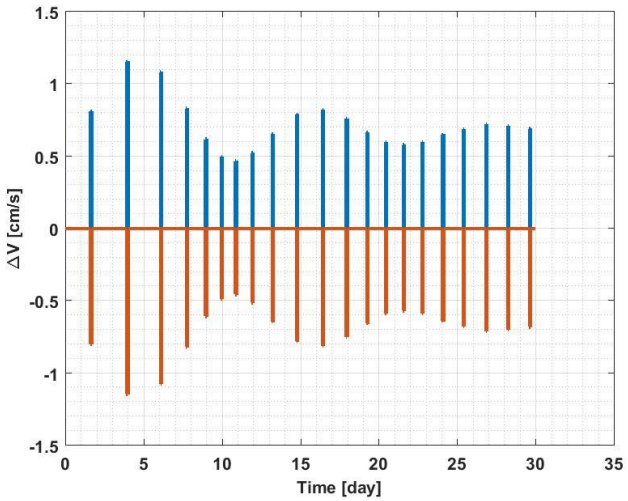

Figure 13: along-track ΔV

5.1.2 Updated TanDEM-X Cluster Flight Algorithm to Match S3NET Requirements

The goal of this section is to adjust the above algorithm to the three satellite configuration: chief and two deputies, as required by the radar mission concept in section 4.3.1. Figure 14 shows a configuration where the chief is 100 km – 200 km before the deputies and the deputies keep a cross-track distance of 1 km between them. The idea is to use the TSX-TDX algorithm to keep the cross-track distance, and apply an additional logic to control the along-track distance between the deputies and the chief. We decided to avoid applying any control manoeuvres by the chief satellite. By doing that we ensure that this new concept can be built on top of an active mission, without interfering with its nominal activities.

Controlling the along-track distance of satellites on similar near circular orbit can be done by introducing small semi-major axis changes. The trigger of this logic will be a violation of the upper/lower bound of the along-track distance between the chief and one of the deputies. Once the trigger is activated, both deputies will apply similar thrust in the along-track direction. If the upper bound is reached, thrust will be applied in the negative along-track direction, and lower bound crossing will activate the opposite manoeuvre. Manoeuvre magnitude should be set to minimum to create a slow along-track drift and save fuel. To reduce the control effort and avoid chattering, we can limit these manoeuvres to one manoeuvre a day. The synchronisation between the two manoeuvres can tolerate a few hundred seconds difference without causing damage to the formation.

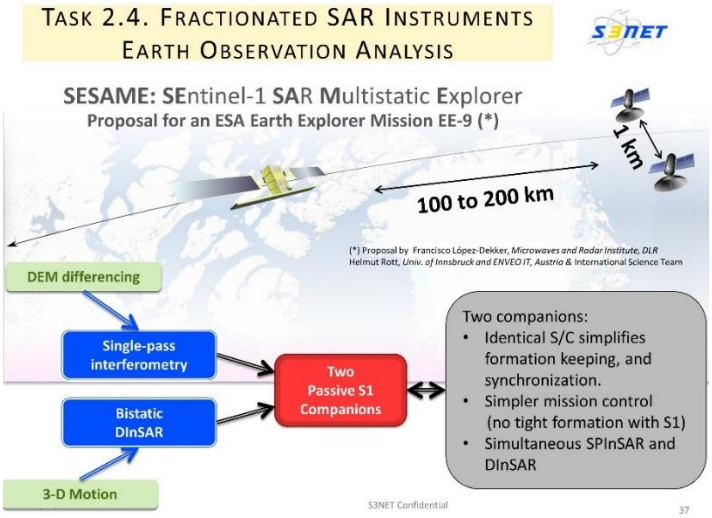

Figure 14: Three satellites configuration consisting of 1 chief and 2 deputies.

While this along-track manoeuvre is required by both deputies, the task of keeping the relative orientation between them can be achieved by applying thrust to only one of the deputies. This will create an uneven fuel consumption over time, but we can alternate between them to balance the fuel consumption. To test this control approach, we use the following parameters for the simulation: the chief mass is 2000 kg, the deputies' mass is 1240, the chief cross-sectional area is 5 m^2 and the deputies' cross-sectional is 3.2 m^2 for the first one and 3.5 m^2 for the second. The simulation duration was set for 1 year. As mentioned before, the chief is not required for any manoeuvre or task other than sharing its navigation solution with its deputies. In this simulation, deputy 2 is performing all the manoeuvres related to the deputies' orientation with respect chief and deputy 1 while deputy 1 is only performing the small manoeuvres related to the along-track distance from the master.

Figure 15 shows the deputies cluster on 3 different planes. We see that the cross-track radial separation is in an ellipse shape meaning no chance of collision. Figure 16 shows the accumulated ΔV of the two deputies. Deputy 2 needs a ΔV of 530 cm/s while deputy 1 needs a ΔV of 100 cm/s. To keep this tight formation, deputy 2 needs to apply thrust every 4 days while deputy 1 applied thrust only 5 times during the year. Figure 17 shows the cross-track distance between the deputies and the chief. We see that the control manages to create about 800 m of separation between them, and the

maximum separation is achieved over the ascending node. In Figure 18 we see that the control keeps the deputies along-track distance from the chief within the required bound of 100 km – 200 km.

The fact the deputy 2 utilizes much more ΔV than deputy 1 might cause mass difference between them, thus increasing the differential drag effect. To reduce this effect, we can alternate the "active" deputy during the mission by ground or autonomous commands.

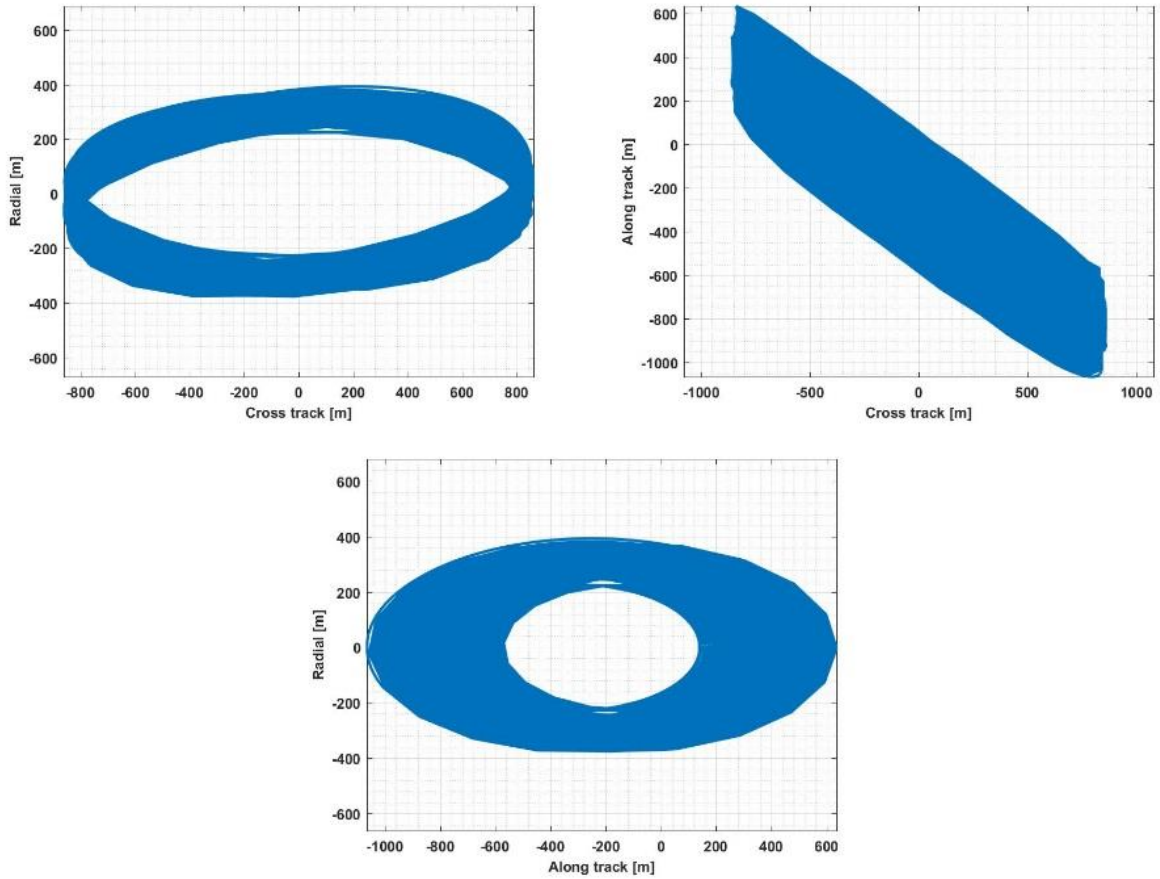

Figure 15: View of the deputies' formation from 3 different planes

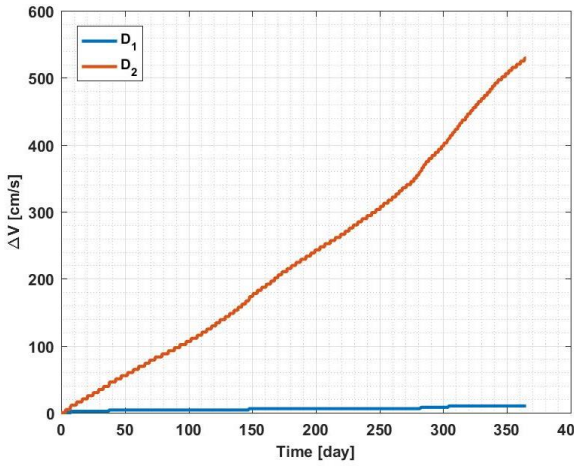

Figure 16: Along-track ΔV

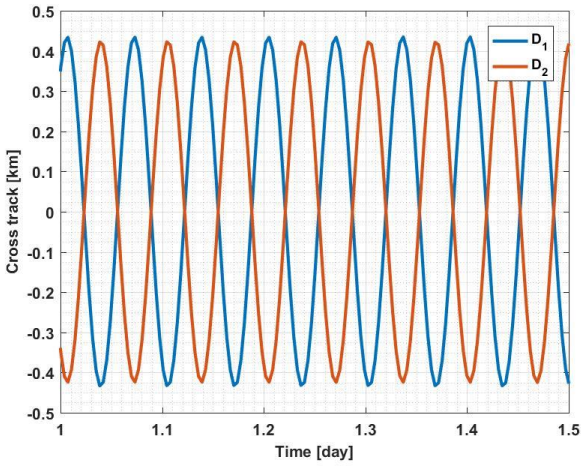

Figure 17: Deputies to chief cross-track distance

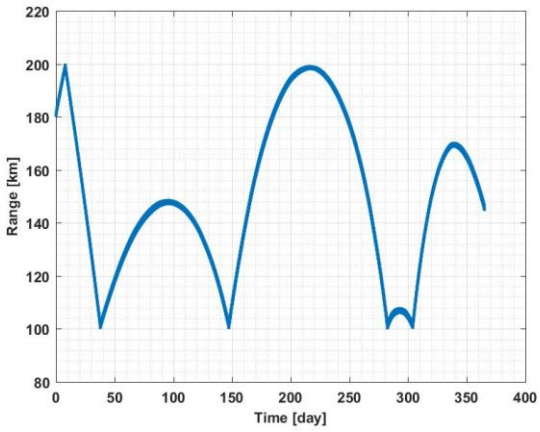

Figure 18: Deputies to chief along-track distance

5.1.3 Orbit Establishment

This section will provide an estimate of the required ΔV for the orbit establishment. Let us assume that the chief satellite is already in orbit for several years. We wish to add two deputies to the same orbit to increase the product value. The deputies injected into orbit with the same orbital elements as the chief but with 1° offset in the true anomaly. The offset creates an along-track distance of 120 km between the chief and the deputies. Let us also assume a 0.001° offset in the true anomaly between the deputies, creating 120 m along-track distance between them. This distance will ensure safe travel until a cluster is established.

We wish to create a 300 m radial distance and 1000 m cross-track distance between the deputies with respect to the chief orbital plane. There is more than one way to create the required radial distance. We can apply thrust in the radial direction, tangential direction or a combination between them. The tangential direction requires less fuel, but has a side effect of creating unwanted semi-major axis difference that will later create an along-track drift that needs to be reduced. The radial manoeuver requires twice as much ΔV, but has no effect on the SMA. In this study we assume radial manoeuver to avoid the along-track drift and also to use as "worst case scenario". This radial manoeuver is optimal on the ascending node. We can also split the manoeuver between the

ascending and descending node, it might be beneficial when dealing with non-ideal thrust. We should also split the manoeuver in half between the two deputies so the cluster symmetry plane will be the chief orbital plane. We used the same simulation parameters as before to test these manoeuvers and the results can be found in Figure 19. The manoeuvers create the required cluster and keep a safe distance throughout the manoeuver. The total ΔV (per satellite) in this case is 71.8 cm/s.

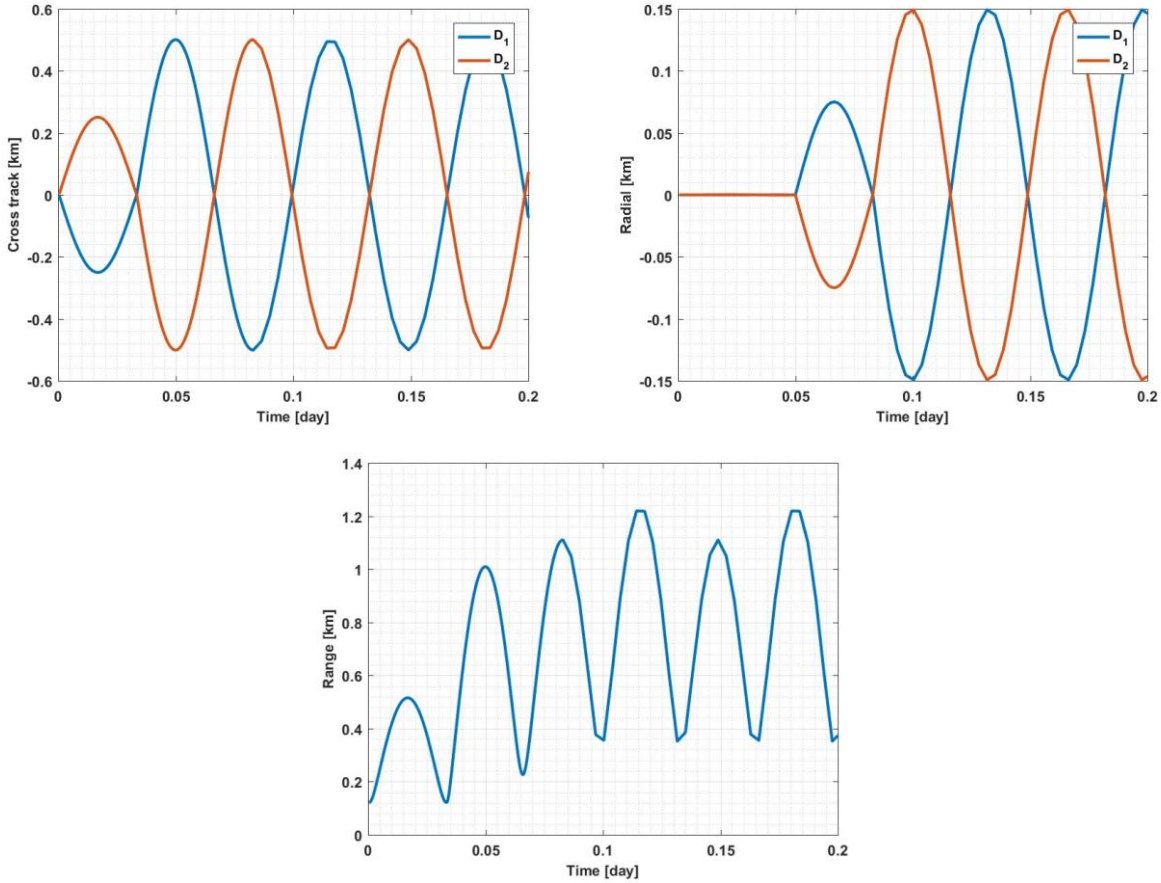

Figure 19: Cross-track, radial and range of the deputies with respect to the chief orbital plane

5.1.4 Orbit Determination

To fulfil the formation flying requirements in section 4.3.2.4, S3NET satellites should use advanced orbit determination algorithms. GPS receivers are considered as a primary tracking system for orbit determination in many satellite missions. A single frequency GPS receiver provides measurements with errors of a few meters. If the distance between two satellites is less than 10 km the knowledge of the relative position is much better, in the order of a few cm.

Using dual-frequency GPS receiver improves the relative position accuracy to a level of 1-3 mm (Ju, 2009) (Gurfil, 2008), which usually needs to be ensured on-ground for supporting the evaluation of payload data to best possible accuracy. E.g., precise baseline determination (PBD) in the order of 1-2mm was required to reach the TanDEM-X mission goal to generate DEMs of 2m relative and 10m absolute height accuracy (Hueso González, et al., 2012), (Wermuth, König, Moon, Walter Antony, & Montenbruck, 2014). For this purpose double differential GPS (DDGPS) processing of carrier phase measurements between both satellites is required using also a Kalman filter. An inter-agency comparison of different softwares/algorithms revealed the standard deviation of relative position

estimates in the order of 1mm in all directions (radial, tangential and cross-track). In an absolute sense, the evaluation of TanDEM-X calibration data takes determined constant offsets of the helix-formation parameters of +6mm and -8mm in radial and cross-track directions for the 20km formation and below 3mm for the close bistatic formation of few hundred meters (Walter Antony, et al., 2013).

5.1.5 Summary

The above method is an alternative for the formation flying algorithm of the S3NET project, mostly for the SAR mission concept suggested by DLR in section 4.3. The control concept of the TSX-TDX mission combined with some additional logic can maintain a formation of chief and two deputies for a long period of time. The estimated ΔV for the formation keeping part will be around 600 cm/s per year for both deputies. For the formation establishment we should add additional 200 cm/s ΔV for both deputies. This technique can also be used to change the cluster baseline during the mission, but the ΔV cost will be significant. The exact cluster parameters need to be optimized for the application, which is a task for WP2.

Some advantaged of using this method are

- The main control concept was used on three previous missions: GRACE (Bettadpur, 2006), PRISMA (Montenbruck, 2006) and TSX-TDX (D'Amico S. a., 2006) and results of these missions can be found on the literature (D'Amico, 2013)
- The control law is simple to implement on a real time system and the required computational power is low.
- The communication burden is low and synchronization between the satellites does not need to be accurate.
- No changes need to be done in the chief satellite and no manoeuvres are required from it. The two deputies can be launched in a later phase improving the product portfolio.

6 PRELIMINARY ASSESSMENT OF ON-BOARD COMPUTATIONAL REQUIREMENTS

This section evaluates and rates the computational requirements for the optical application scenarios described in section 3 and for the radar use cases described in section 0. Estimations with regard to computational complexity is described in the following sections, where the number of FLOP (FLoating point OPerations) is used in order to indicate the complexity.

6.1 Assessment for Optical Applications

6.1.1 Assessment for Cloud Detection Algorithm

For the cloud detection algorithm described in section 3.2 the total number of Floating-Point operations (FLOPs) is computed considering an image whose size equals 'N' rows and 'M' columns. The top of atmosphere radiance phase mainly consists in multiplying a scalar to a matrix (i.e. the acquired image). The number of FLOPs is equal to:

$$\text{FLOPs}_{top-of-atmosphere} = N * M * n\_bands$$

Where 'n_bands' stands for the total number of spectral bands. The resulting image is then classified using the scalar product derived from the SVM classifier, plus a fixed parameter '*b*'. The size of the SVM weight vector is related to the number of spectral features used to classify the image:

$$\text{FLOPs}_{classification} = N * M * (2 * n - 1) + N * M + N * M$$

Where '*n*' stands for the total number of spectral features. The first part of the equation corresponds to the computational cost of applying the scalar product. The second part is the cost related to a scalar added to a matrix (i.e. '*b*'). The final part of the equation corresponds to a comparison operation, and thus the detection of cloudy pixels.

Finally, the last refining part can be summarized as a convolution followed by an additional comparison operator. The total number of FLOPs is:

$$\text{FLOPs}_{refining} = N * M$$

The described cloud detection algorithm can be highly parallelized to improve the computational performances. Furthermore, the total number of FLOPs can even be reduced applying the processing on a shrunk image. This latter is obtained by applying a 4x4 minimum window kernel over the original image. It has been noted in literature that the algorithm still ensures good detection performances, while at the same time significantly reducing computational requirements.

The proposed algorithm in section 3.2 is applied to the Sentinel-2 case in order to understand approximately the total number of FLOPs. The total number of FLOPs equals to almost 1.5 millions. The cloud detection algorithm, in case of Sentinel-2 data, must complete the detection in less than 1.7 seconds, which is the acquisition rate of the satellite. Thus the minimum required computational speed would be 0.882 MFLOPS, plus the possible overheads related to data transfers, etc.

The complexity of the algorithm is concentrated in the training phase of the SVM classifier, which is done just once. Reusing of the results is quite cheap from a computational standpoint. The classifier can be trained during the in-flight commission period, as suggested by (Camarero, Thiebaut, Dejean,

& Speciel, 2010), and re-training could be done once in a while to incorporate slight changes in the instrument characteristics due to aging.

The application of cloud mapping does not necessarily require acceleration by a space grade DSP processor. Current European Microprocessors such as Gaisler LEON3FT might be able to guarantee a sustainable streaming (the LEON3FT is limited to about 200 MFLOPS). Still, as the number of spectral bands (in case of hyperspectral imaging) or the required resolution (high-resolution imaging) increases for a mission such a processor might meet its limitations. Furthermore cloud mapping represents only an auxiliary task in spaceborne imaging in order to reduce the data storage and downlink requirements for any kind of optical imaging. Therefore, it can be expected that further compute capabilities will be needed in order to process other algorithms. An offloading to a DSP accelerator should be considered.

6.1.2 Assessment for Image Compression Algorithm

This section investigates the computational requirements for the CCSDS image compression algorithm of section 3.3, in particular the prediction phase. In the following part, the sub-operations are listed and considered in terms of FLOPs. In order to understand the following formulas, we indicated as $s_{z,y,x}$ the sample of the image in the band z, row x and column y, while P, as already explained, is the number of previous bands considered in the prediction.

a) Local sum computation. First of all, the local sum $\sigma_{z,y,x}$ of the neighboring samples is computed. Two ways are available to make this computation: neighbor- or column-oriented. These two ways are selected by the input parameter *Local sum mode* mentioned in Table 2 that is typically set as *Neighbor* oriented in case of *full prediction mode* operation (that is the most computationally demanding mode ensuring greater performances). This case is analysed here.
For this case, the local sums are computed by the formula indicated in the left column of the following Table 7. The right column indicates instead the number of elementary operation (FLOPs) needed to perform the local sum (3 adders needed) for each input sample $s_{z,y,x}$

Operation	# FLOPs
$s_{z,y-1,x-1} + s_{z,y,x-1} + s_{z,y-1,x} + s_{z,y-1,x+1}$	**3**

Table 7: Local sum formula and related # FLOPs

b) Local difference computation. Two kinds of local differences are computed in the *full prediction case*:

a. **Central Local Differences (CLD)** $d_{z,y,x}$: a central local difference variable is computed for all the P previous band by means of the formula listed below. Since the reported formula has to be applied P times (for the number of previous bands), this results in the FLOPs number indicated in the right column of the following Table 8. Each computation requires 2 FLOPs (A product and a sum) for each input sample $s_{z,y,x}$ and for each of the P bands.

CLD for the generic $z - i$ band	# Total FLOPs (for all P bands)
$d_{z-i,y,x} = 4s_{z-i,y,x} - \sigma_{z-i,y,x}$	2P

Table 8: Central Local Difference (CLD) formula and related # FLOPs

b. **Directional Local Differences (DLD)** $d^N_{z,y,x}$, $d^W_{z,y,x}$, $d^{NW}_{z,y,x}$. These are the differences computed along the space axis of the image and are used (and computed) also in case of *Full prediction mode* here treated. N, W, NW stand thus for north, west and north-west, and indicate the "direction" in which differences are computed with respect the current image sample. Follows the formula for each of the directional difference and FLOPs needed (2 FLOPs per each computation: a product and a sum).

DLD	# FLOPs
$d^N_{z,y,x} = 4d_{z,y-1,x} - \sigma_{z,y,x}$	2
$d^W_{z,y,x} = 4d_{z,y,x-1} - \sigma_{z,y,x}$	2
$d^{NW}_{z,y,x} = 4d_{z,y-1,x-1} - \sigma_{z,y,x}$	2

Table 9: Directional Local Difference (DLD) formula and related # FLOPs

In order to feed the next algorithm block, the predictor, each of the previous term (in full prediction mode) is **multiplied** by a proper weight factor. These factors are changing at every iteration basing on the value obtained by the residual computation performed for the previous sample. So, the total number of FLOPs becomes:

Operation	# FLOPs
$Weighted\ CLD$	**4P**
$Weighted\ DLD$	**12**

Table 10: Total # FLOPs for Weighted CLD and DLD

c) **Prediction Residual (PR) computation**. This is done based on the computed local differences (both central and directional in Full prediction mode). The prediction algorithms used in in CCSDS compressor is based on adaptive Filtering, i.e. a filter that adapts its coefficients iteratively. From this point of view, focusing on the FLOPs computation, the filter can be considered as a sum of the previously computed weighted CLD and DLD multiplied by a factor: i.e. a sum of products. The residual computation is instead a simple subtraction operation and thus results in 1 single FLOP.
For each sample of the image to be compressed the following Table 11 indicates the resulting number of FLOPs.

Operation	# FLOPs
$Adaptive\ Filtering$	(P+3)+(P+3)=**2(P+3)**
$Residual\ Computation$	**1**

Table 11: Total # FLOPs for Prediction Residual (PR) computation

Finally, it is worth noticing that the above operations have to be **repeated** $N \times M \times n\_bands$ times (Being $N$and M the size of the image, and n_bands the number of bands) i.e. for each sample of the input image to be compressed.

The final number of FLOPs needed by the algorithm described in section 3.3 is expressed as:

$$\boldsymbol{FLOPs_{tot}} = N \cdot M \cdot n\_bands \cdot [3 + 4P + 12 + 2(P+3) + 1] =$$

$$\boldsymbol{N \cdot M \cdot n\_bands \cdot [22 + 6P]}$$

In order to make the final count for a real case of Sentinel-2 data, we assume the value of P=3, referred as optimal for the compression rate by the authors of (Santos, Berrojo, Moreno, J., & López, 2016). In this way we obtain:

$$\boldsymbol{FLOP_{\{tot\}} = 40 \sum_{i=1}^{13} N \cdot M},$$

since the resolution, and thus the number of pixels, in general differs for each spectral band of Sentinel data.

In order to obtain the final result, it is worth keeping in mind (see https://directory.eoportal.org/web/eoportal/satellite-missions/c-missions/copernicus-sentinel-2 for details) that:

- **Each** level-0 products is composed by almost **12 *"granulates"***
- **Each** granulate cover a swath of $\boldsymbol{25\ Km \times 23\ Km}$ (the last dimension correspond to the longitudinal one)
- **The spatial resolution is:**
  - **10 m for 4** among the 13 bands
  - **20 m for 6** among the 13 bands
  - **60 m for 3** among the 13 bands
- That means that **each granulate** has almost
  - $2500 \times 2300 = 5.75 \cdot 10^6$ **Samples** for each of the **4 band** of 10 m resolution
  - $1250 \times 1150 = 5.4375 \cdot 10^6$ **Samples** for each of the **6 band** of 20 m resolution
  - $417 \times 384 = 160.128 \cdot 10^3$ **Samples** for each of the **3 band** of 60 m resolution.

Finally we can, thus, compute an approximate number of FLOPs for each granulate as:

$$\boldsymbol{FLOP_g = 40\left(4\left(5.75 \cdot 10^6\right) + 6\left(5.4375 \cdot 10^6\right) + 3\left(160.128 \cdot 10^3\right)\right) = 2.24 \cdot 10^9\ FLOPs},$$

that for a single image (almost 12 granulates) gives the following total number of flops:

$$\boldsymbol{FLOP_{single\ image} = 26.88 \cdot 10^9\ FLOPs}.$$

Considering that a new image is acquired approximately every 1.7 seconds, in order to compress a single Sentinel image the system has to support a speed of almost:

$$\boldsymbol{15.81 \cdot 10^9 \frac{FLOPs}{sec}}.$$

$\boldsymbol{16 \frac{GFLOPs}{sec}}$ may seem quite a big computing throughput. This is not completely true as some operations are very simple (for instance the multiplication of a number for a factor of two simply translates into shift operations at the hardware level, and so on). At the expense of more intense memory usage and internal resources consumption, with a proper number of pipe stages for parallelization, this implementation is feasible for FPGAs powered with hundred-MHz clock.

This Application - without any doubt - requires acceleration by a high-performance processor / DSP / or FPGA. Even a theoretical computation evaluation gets to the result that the computational complexity in real-world scenarios is beyond the capabilities of common space-grade multi-core processors like LEON3FT.

Even for high-performance DSPs already available or available in near future this represents a compute task on the edge of a single DSP/processor capabilities, since we can't assume a close to

100% compute utilization for this kind of algorithm. Therefore a multi-processor solution will be needed in order to solve jobs like for the Sentinel-2 mission. Scaled down mission scenarios for micro- or nano-satellites might only require a single high-performance DSP. For even more demanding scenarios like Sentinel-2 the project needs to estimate and parameterize the required compute system scalability.

6.1.3 Assessment for Band to Band Registration Algorithm

In the following, the computational load is computed and reported for each processing block of the optical band registration algorithm described in section 3.4 . We define:

P → generic pixel (x, y)

M → # of image lines

N → # of image columns

$\boldsymbol{n\_bands}$ → # of image bands

The number of FLOPs for each step of the algorithm is given below.

GRADIENT IMAGE GENERATION

The general formula for two-pixel gradient is:

Formula: $Grad: | P_{i+1,i} - P_{i-1,j} | + | P_{i,j+1} - P_{i,j-1} |$

The total number of FLOPs for this operation, when performed on the entire image can be estimated as follows:

Total # of operations ≈ N * M * (n-bands - 1) * 5;

Where the fixed coefficient 5 is the number of operations to be made for each pixel on each band, i.e. two differences, plus two absolute values, plus one sum.

PHASE CORRELATION

The following basic steps are foreseen:

- Fast Fourier Transformation of both considered bands
- Pixel-by-pixel multiplication of the two transformed images
- Division of the result by the absolute value of the multiplication of the two transformed images (normalization)
- Inverse Fast Fourier Transformation of the previous result
- Location of the maxima in the inverse transform result

The Radix-2 method proposed by Cooley and Tukey (Cooley & Tukey, 1965) is a classical algorithm for FFT calculation. Due to high computational complexity of FFT, higher-radix algorithms such as radix-4 and radix-8 have been proposed to reduce **computational** complexity. On the other side, for real-time applications, such as satellite applications, hardware implementation of FFT is interesting.

Owing to its simplicity, radix-2 is a popular algorithm to implement FFT. Radix-2^p algorithms have the same order of computational complexity as higher-radix algorithms, but still retain the simplicity of radix-2. Results from (Amirfattahi, 2013) show that radix-2^2 have significantly lower computational complexity compared with radix-2. For computing the number of real multiplications (flop) we use the radix-2^2 FFT approach. The formula is the following, with P the number of pixel to be computed:

$$\textbf{Total cpu operations} \approx (P): \left(\frac{9}{4} \cdot P \cdot \log_4 P - \frac{43}{12} \cdot P + \frac{16}{3} \right) \cdot \text{n\_bands} \quad \text{P= M x N}$$

Then the cross-power spectrum of the two images is derived in the form of a same-sized matrix CPS.

To multiply the FFT-ed bands, the required number of operations is:

Formula: $$\text{CPS} = \frac{Matrix\ A \times Matrix\ B}{|\ Matrix\ A \times Matrix\ B\ |}$$

Total # of operations ≈ 2 x M x M x N x ($\_bands$ - 1)

The inverse Fourier transform is then applied to CPS, which yields the spatial offset in the spatial domain. This requires the same number of operations as the direct FFT.

$$\textbf{Total cpu operations} \approx (P): \left(\frac{9}{4} \cdot P \cdot \log_4 P - \frac{43}{12} \cdot P + \frac{16}{3} \right) \cdot \text{n\_bands}$$

VALID REGISTRATION

The computational load for the first validation criteria (the Euclidean distance) is:

Total # of operations ≈ 10 x (b-1)

The coefficient 10 comes from an estimate of the operations needed to implement the above computation, and is not to be taken as a precise value.
For the second criteria, the worst case is considered: the distance is tested on all relevant pixels.

Total # of operations ≈ M x N x 10 x (b-1)

SUB-PIXEL ESTIMATION

Total #of operations ≈ 20 x (n_bands - 1)

IMAGE REGISTRATION

Total cpu operations ≈ M x N x 6 x (n_bands - 1)

The global number of operations is shown on the graph below and it represents the total number of basic operations needed to process a two-band dataset whose total number of pixels is reported on the horizontal axis. In the general case of n_bands > 2, the number on the vertical axes in Figure 20 is to be multiplied by (n_bands - 1) as each new band requires a single new processing operation set.

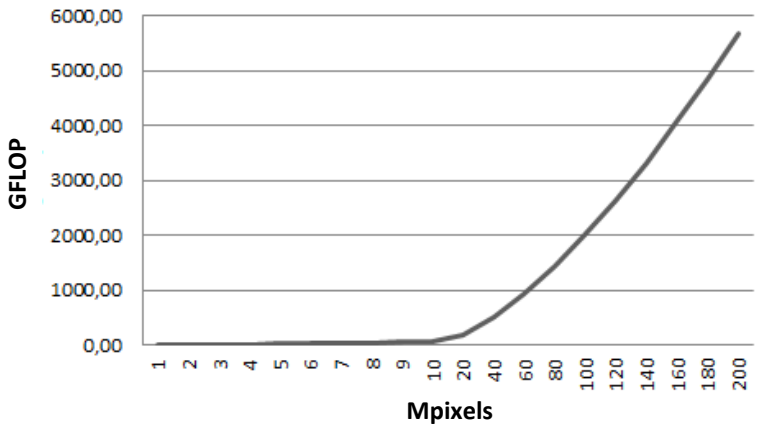

Figure 20: # of floating point operations versus total # of pixels for the registration algorithm using 2 bands.

As a reference, for a dual-band image sized like single Sentinel-2 granulates, the overall computational load sums up to around 135 GFLOP. Although we can assume a relatively high compute utilization due to mostly regular and independent computation schemes, such on-board image processing job can only be performed by either a dedicated hardware implementation or leveraging multiple high-performance processors in parallel. Band-to-Band Registration represents the most performance critical optical imaging routine selected for S3Net and therefore requires special attention.

6.1.4 Conclusions for Optical Algorithms

In the context of the S3NET project, a computational analysis has been carried out on the three optical image processing algorithms suggested in report D1.1. These algorithms have been selected after a deep analysis of the literature and results from the combination of two independent needs: on the one side, that the application is desirable from the user's standpoint and, on the other side, that the application fits into the limited on-board available resources. Three applications were finally selected: **cloud detection**, **band-to-band co-registration** (**BBR**), and **image compression**.

Each application, and in particular, the implementation proposed by literature references, has been deeply investigated. For every application, the proposed algorithm has been split into elementary blocks, which have been analyzed in terms of elementary operations i.e. FLOP (for further details see section 6). In order to get a numerical feeling of the results on a real case, the number of FLOPs resulting by the execution of the three algorithms has been computed in case of Sentinel-2 on-board products.

What emerges from this analysis is that the computational impact of the three algorithms is extremely different from one to another. The final results are reported, for a single Sentinel-2 granulate, in the following list:

- **Cloud Detection →** $1.5 \cdot 10^6\ FLOP$
- **Compression →** $2.24 \cdot 10^9\ FLOP$
- **Band-to-Band registration →** $135 \cdot 10^9\ FLOP$

As one can see, the number of FLOP and consequently the needed hardware complexity has to be accurately evaluated in terms of tradeoff between usefulness of the on-board implementation and related computational cost. At a glance, the band-to-band registration and compression algorithms

are the most demanding in terms of resources. Cloud detection on the other hand, can aid the reduction of calculations spent on compression of representative sized images by up to 3 orders of magnitude depending on the scenario/weather conditions.

6.2 Assessment for Radar Applications

6.2.1 Assessment for Staggered SAR Processing

The on-board processing for the staggered SAR concept of section 4.1 is mandatory to remove the oversampling of the received SAR raw data, which is due to mission constraints. For the Tandem-L mission proposal the oversampling factor is between 2 and 3. The processing must perform first an alignment of the range lines followed by a digital FIR filter applied to the azimuth direction. The peculiarity of this FIR filter is the demand for varying coefficients, which repeat every 300 range lines. In addition, the set of coefficients must be updated with range. For the estimation of the computational demand it is assumed that the radar timing is such that the range alignment can be performed by integer sample shifts (with negligible effort). Then the application of the FIR filter dominates the calculation and requires the following number of operation,

Total cpu operations ≈ M/*osf* x N x (7 x *n_coeff – 1)*,

where N is the size of one range line, M is the number of range lines prior to filtering*, n_coeff* are the complex valued coefficients of the FIR filter and *osf* is the oversampling factor. Assuming a FIR filter length of 20 samples for a wide coverage **Tandem-L scene** of 350km by 350km and oversampling factor of 3, the resulting computation count is in the order of **830 GFLOP**. This rough estimate doesn't take into account the computation of the coefficients, which is a factor of 1000 lower count (and therefore negligible), as they repeat periodically.

Another challenge is to handle the large amount of 33 GByte of raw data, which are generated by the sensor for each scene at a rate of roughly 700 MByte/sec (or 5.6Gbit/s). These data rates will most likely require the splitting of the data stream onto multiple processors. It is clear that such an amount of data cannot be routed through a bottleneck such as a management core like LEON3FT that certainly doesn't deliver necessary I/O bandwidth. If a corresponding benchmark needs to be conducted a host needs to be set up that can distribute data among multiple processors in order to emulate the partitioning.

6.2.2 Assessment for SAR Image Formation

The challenge for SAR image formation processing will be most likely to efficiently perform memory/data transactions, since most processing steps consist of FFTs. The compute complexity of the algorithm described in section 4.2 will be as low as O(N)=N log(N), where N is the number of (complex) samples.

Still, although the bottleneck will be memory bandwidth (e.g. to off-chip DDR memory) also compute performance needs to be matched. Assuming e.g. an efficient complex-value Radix-4 FFT algorithm the following number floating point computations needs to be performed:

N = number of samples

B = number of butterflies = N/4

S = number of FFT stages = lg_4 (N)

C_B = number of computations per butterfly ~ 44

C_S = number of computations per stage = C_B*B = 42 * N/4 = 11 * N

T = total/overall number of computations = C_S * S = = C_B*S= 11 * N * lg_4 (N)

The Application "Generation of focused, high resolution (bistatic/generic) SAR images" with its 6 1D-FFT steps will therefore require Y=6*T computations only for FFT processing (i.e. for 4096 points 6.66GigaFLOP and for 16384 points 124.02 GigaFLOP).

Assuming a raw data size of NxM complex samples (range x azimuth), the computational demand is roughly evaluated as follows:

Processing Step	# FLOP
Range FFT	11 *M* N * lg_4 (N)
Matched Filter	6*N*M
Range IFFT(*)	11 *M* N * lg_4 (N)
Range FFT(*)	11 * M*N * lg_4 (N)
Azimuth FFT	11 *N*M * lg_4 (M)
Vector for Interpolation	7*N*M
Stolt Interpolation	100*N*M
Phase Function	9*N*M
Wave Migration	6*N*M
Azimuth IFFT	11 * N*M * lg_4 (M)
Range IFFT	11 * M*N * lg_4 (N)

Table 12: Computational requirements for SAR image formation

The overall processing of one single SAR scene **Sentinel-1 specific stripmap scene** of size 80km by 120km, including all steps of the algorithm, requires approximately **416 GigaFLOP**, from which 330 GFLOP need to be allocated to FFTs. (Depending on sensor parametrisation the intermediate range FFT(*) and iFFT(*) can be omitted, which will save approximately 100 GigaFLOP.) Algorithmic optimisation is worthwhile also for the Stolt Interpolation step, which amounts to approx. 65 GigaFLOP.

It is expected that such application will be most likely limited by memory bandwidth/transfers. If data needs to be written to external memory (e.g. DDR2/3/4 RAM) after each intermediate step, the memory interface (with a bandwidth in the order of 2.5GB/s) will be the bottleneck. If the local external memory per processor allows storing 2-4GB of data and overall I/O can sustain about 1Gbit/s throughput, then a potential solution could be to distribute sequential images onto different processors and allow a private style (independent) processing, since it can be expected that the interface to external memory such as the local DDR RAM allows higher transfer rates than the I/O between processors (e.g. SpaceWire or Ethernet).

6.2.3 Assessment for bistatic Synchronisation

For bistatic SAR image acquired by a formation of SAR sensors, there are additional computational demands as described in section 4.3. However, the conditioning of the synchronisation signal

operates on a much smaller data set, than the recorded SAR echoes from the Earth. The procedure also doesn't need to perform as many FFTs.

Assuming a complex single-look image data size of *N x M* complex samples (range x azimuth), synchronisation signals are assumed to be available every 1000 pulses.

Processing Step	# FLOPs
Range FFT	11 *M* N * lg_4 (N) / 1000
Matched Filter	6*N*M / 1000
Range IFFT	11 *M* N * lg_4 (N) / 1000
Computation of conditioned Sync parameters	M/10

Table 13: Computational requirements for conditioning the bistatic SAR synchronisation

The number of operations corresponding to the Sentinel-1 parameters used in the previous subsection is dominated by the FFTs and corresponds to **130 MegaFLOP**. Efficient algorithm implementation can avoid the IFFT, which may further reduce the already small operation count.

Although even a management processor such as a LEON3FT is capable of handling such data rates, it is recommended that this type of processing is performed on a high-performance processor, since the management core is designated for control tasks that are supposed to not be heavily affect in terms of latency. Handling such low processing demands on high-performance processors that can potentially handle multiple GFLOPS, if not tens of GFLOPS might not even require special optimization techniques. Still for the sequential flow of the application it will be interesting to benchmark this workload, as quite frequently sequential code tends to reduce compute utilization.

6.2.4 Assessment for SAR Multi-looking

Compared to the SAR image formation processing, multi-looking as described is section 4.4 is a cheap application with respect to computational requirements.

Assuming a complex single-look image data size of *N x M* complex samples (range x azimuth), the computational demand in terms of FLOPs is given as:

Processing Step	FLOPs
Detection	3 *N*M
Averaging	N*M

Table 14: Computational requirements for SAR multi-looking

Efficient implementation ensures that the computational costs are independent on the oversampling factor *osf* and the *L* the number of looks. For the Sentinel-1 case this results in approx. **2,5 GigaFLOP** for a standard scene of 80km x 120 km.

Certainly this workload can be executed on a capable high-performance processor and does not necessarily require distributed computing. Still the execution time for representative detection algorithms needs to be evaluated/measured in order to estimate performances and hardware demands for future missions.

6.2.5 Conclusions for Radar Algorithms

The computational analysis has carried out for the four radar data processing algorithms suggested in report D1.1. These algorithms have been selected as they are mandatory or desirable to support proposals for future SAR missions. Two of the algorithms (staggered SAR and SAR image formation) pose challenging requirements for on-board computational requirements. The other two algorithms (synchronization and multi-looking) have low to moderate computational complexity. They cannot be treated as stand-alone as they must be considered in support of the bistatic SAR image formation or as a data compression alternative.

Each algorithm has been analyzed in terms of elementary operations i.e. FLOP. In order to get a numerical feeling of the results on a real case, the number of FLOP resulting by the execution of the three algorithms has been computed for the cases of wide swath Tandem-L staggered SAR Doppler filtering and for stripmap Sentinel-1 bistatic SAR image formation.

What emerges from this analysis is that the staggered SAR processing concept is considered too ambitious for the implementation within S3NET, taking also into account that it does not necessarily relate to a formation flying mission. However, the other three radar algorithms will be considered for further evaluation within the project.

7 PRELIMINARY ASSESSMENT OF COMMUNICATION REQUIREMENTS

The following sections describe preliminary assessments of communication requirements. Those assessments are based on the optical application scenarios (see chapter 3) and radar use cases (see chapter 0). The architecture and preliminary design of the S3NET communication simulation system described in delivery D1.4 are derived from the preliminary assessments of communication requirements. In addition those requirements will define the specification of the S3NET communication simulation system in delivery D4.1.

7.1 Assessment for Optical Patchwork Formation Mission

The panchromatic applications, which include ship detection & type identification and homeland security, don't use any inter-satellite-links, except for the case of autonomous formation flying. But the relative time precision and time synchronization between the platforms should be at least in the order of magnitude of 1 ms to allow a correct overlapping of the acquired images. Therefore a synchronization scheme that includes a direct point-to-point communication between the satellites should be evaluated. A time division multiple access techniques (TDMA), which allow several satellites connected to the same multi-point transmission medium to transmit over it and to share its capacity will take advantage of this synchronization.

For the uplink and downlink of the TC, TM and payload data are approximate 10 minutes available. Considering the data amount and number of satellites the required throughputs for the payload downlink is 300 Mbps. The bandwidth for near earth satellite in the X-band is 0.5 GHz for uplink and downlink. Considering a modulation technique with a small spectral efficiency of 1 such as binary phase shift keying (BPSK) a data rate of 500Mbps can be achieved. For the TC uplink and TM downlink the bandwidth of 10 MHz from the S-band resulting in a data rate of 10Mbps using BPSK is sufficient.

7.2 Assessment for Optical Spectrum Fractionation Mission

In the spectrum fractionation application the images of the single satellites are acquired using a different set of spectral bands (VIS, SWIR, NIR). The image of a certain AOI from the different satellites are correlated and overlapped with the help of precise geo location information instead of a time stamp. Therefore the synchronization requirements are relaxed (1 second), since they are based on the dynamic of the observed area.

In comparison to the panchromatic optical applications the available time for data transmission is increased, but also the amount of data is increased. This leads in a comparable required data rate and therefore a similar communication technique is advisable.

7.3 Assessment for Staggered SAR System Concept

The staggered SAR use case is related to the Tandem-L mission. The requirements for the uplink are relaxed since only a low data rate of 64 kbps for TC and 128 kbps/2 Mbps (programmable) for TM is needed. This throughput is needed in a time window of 10 minutes, where the satellite is visible from the ground station. Communication via S-band and BPSK is sufficient.

The download is currently planned to be realised via Ka-band. In general the Ka-band offers a very high bandwidth (uplink 3.5 GHz, downlink 1 GHz) and therefore data rate. However, electromagnetic signals within this range of 30 GHz get absorbed by water vapour/rain. Therefore the usage of the Ka-band is not recommendable for tropical regions. Compared to the X-band the Ka-band antennas can be much smaller due to the short wavelength (~1 cm), but also the transmission power needs to be increased to achieve a sufficient range and quality of the signal. On the other hand the small spot beams allow multiple frequency re-use (multiple access) in a swarm without adjacent satellite interference.

7.4 Assessment for Radar Formation Flying Mission

The second SAR use case group is based on the Sentinel-1 mission, a polar orbiting two-satellite constellation. The proposed formation includes high-speed ISL communication.

For the uploading of DEM updates for a tile of 200km by 200km at 30m resolution, the data amount is estimated to be 85 MByte. This amount of data needs to be uploaded within 10 minutes resulting in an upload data rate of 1.2 Mbps, which is achievable using S-band and BPSK.

The download link for the payload data requires a data rate of 86 Mbps per satellite in case of no on-board processing and 35 Mbps per satellite if on-board processing (image formation + multilooking) is performed. In both cases the throughput can be satisfied by a X-band BPSK communication link.

The intra-satellite transmission uses either raw data or high resolution SAR images. Therefore one data take is 1.5 GByte in case of raw data and/or 4.8G Byte in case of processed L1A data (single-look complex). Considering 17 sec recording time, a data rate of 700 Mbps and/or 2.1 Gbps, for raw or processed data respectively is required for operation with constant latency. The data type for raw data is “8-bit integer” and for image data “single precision float”. Due to the high-speed ISL requirement for L1A data an optical inter-satellite link may be considered as an option. A free-space laser link allows higher data/power efficiency, which is important for power-limited systems like a satellite. This advantage is generated by the fact that laser beams are much more directive than a high divergent radio wave. The same characteristic introduces relaxed requirements regarding multiple access, since signals are not omni-directional broadcasted and interfere other receivers. The drawback of the system is the need for extreme precise pointing of the laser beam. To overcome this limitation, the S3NET concept suggests to restrict the data exchange to raw data level or drop the constant latency requirement, such that inter-satellite communication can be accomplished by a low power X-band BPSK communication link. Image generation processing, as well as any other subsequent processing can be performed jointly on the receiving chief or deputy. A benefit is that no downlink needs to be foreseen or operated for the sending deputies.

In bistatic formation flying for SAR applications the recorded data from the receiver (slave/deputy satellite) needs to be synchronized in time and phase with the master (chief) satellite. The compensation of the relative clock frequency offsets and different timing references of the systems is mandatory to avoid a significant increase in the data rate and errors in the image processing. This can be realized by defining hard requirements regarding latency and/or by annotating a timestamp and position data (GPS) to the sensor data to enable synchronization.

8 CONCLUSIONS

Fractionated optical and radar missions require different algorithms for on-board data processing, safe formation flying concepts, and different communication demands. These requirements have been assessed in this report in order to restrict the follow-on detailed mission and algorithm study to a representative subset and to allow the dimensioning of the S3NET compute system and the S3NET communication simulation system to be developed in this project.

Two fractionation concepts for optical EO have been proposed in this report: **patchwork** to cover a wider area with high resolution and **spectrum fractionation** to increase the number of spectral bands. For supporting these applications three algorithms were identified as being beneficial for on-board processing: **cloud detection, image compression and band to band registration**. The detailed investigations performed with respect to computational complexity revealed the need for multi-core DSP processing, especially for the compression and registration algorithms.

With respect to the radar use cases, the **staggered SAR concept** and the **bistatic SAR imaging** where selected for an assessment of on-board computational demands. The Doppler filtering approach inherent to the Staggered SAR concept turned out to be relatively simple in concept, but extremely demanding with respect to data throughput, in particular when assuming the Tandem-L mission scenario. Within S3NET it will not be investigated further. Instead generic monostatic and bistatic **SAR image formation** is rated as being of more general interest. It was found of similar computational complexity as the optical image compression and registration. The demand for multi-core DSP processing is therefore also given in this case. For reducing the downlink requirements, **multi-looking** is suggested for implementation as part of the follow-on work packages of S3NET, although it poses only modest computational requirements, similar as the **conditioning of the synchronisation signal**.

To complement the requirement analysis **the inter-satellite** and **downlink communication demands** were collected and analysed for both optical and radar application scenarios. It was found that for all proposed use cases sufficient downlink capacity can be achieved with state-of-the art microwave technology. An exception is the Tandem-L mission scenario, which is at the limit of Ka-band technology, but which will not be further discussed in S3NET. It is also suggested that those mission concepts shall be prioritized in the follow-on project stages, which do not make use of optical inter-satellite laser links. In particular there is no strict requirement for transferring complete full-resolution complex SAR data between satellites or to the ground.

This report also includes a first assessment of **formation flying feasibility** for the particular case of the suggested bistatic SAR formation mission. An extension of the formation flying concept used for the TanDEM-X mission was proposed, taking into account the proposed radar formation consisting of one chief and two deputies. The presented approach was shown to be within the fuel budget limits of a typical satellite mission. A similar feasibility analysis will be performed also for the two proposed optical formations as part of the follow-on mission analysis phase of the project. In addition, the presented SAR analysis needs to be refined, taking into account the consolidated orbit choice, different formation options and the satellites' dimensions and mass.

From these first requirement analyses, it seems that the identified **optical and radar** use cases pose **similar computation requirements**. This is a benefit for the development of the S3NET hardware

demonstrator, i.e. the S3NET concept compute system in WP3 and of the S3NET communication simulation system in WP4. However, for ensuring the support for a variety of missions, a scalable on-board system infrastructure shall be designed, with more detailed and specific requirements to be collected during the algorithm and mission effectiveness study in WP2.

9 BIBLIOGRAPHY

Albinet, M., Camarero, R., Isnard, M., Poulet, C., & Perret, J. (2013). Improving multispectral satellite image compression using onboard subpixel registration. In. *SPIE Optical Engineering+ Applications* . (pp. 887106-887106). International Society for Optics and Photonics.

Amirfattahi, R. (2013, Oct-Dec). Calculation of Computational Complexity for Radix-2p Fast Fourier Transform Algorithms for Medical Signals. *J Med Signals Sens., 3*(4), pp. 217–224.

Bachmann, M., Borla Tridon, D., De Zan, F., Zink, M., & Krieger, G. (2016). Tandem-L Observation Concept - An Acquisition Scenario for the Global Scientific Mapping Machine. *EUSAR.* Hamburg, Germany: VDE.

Bettadpur, O. M. (2006, Oct). E/I-vector separation for safe switching of the GRACE formation. *Aerospace Science and Technology, 10*, 628--635. Retrieved 09 14, 2016, from http://dx.doi.org/10.1016/j.ast.2006.04.001

Camarero, R., Thiebaut, C., Dejean, P., & Speciel, A. (2010). CNES studies for on-board implementation via HLS tools of a cloud-detection module for selective compression. *SPIE Optical Engineering+ Applications* (pp. 781004-781004). International Societyfor Optics and Photonics.

Cooley, J. W., & Tukey, J. W. (1965). An algorithm for the machine calculation of complex Fourier series. *Math Comput., 19*, pp. 297–301.

Cumming, I., & Wong, F. (2005). *Digital Processing of SAR Data.* Norwood, MA: Artech House.

Curlander, J. C., & McDonough, R. N. (1991). *Synthetic Aperture Radar: Systems and Signal Processing.* New York: John Wiley & Sons.

D'Amico, S. (2010). *Autonomous formation flying in low earth orbit.* TU Delft, Delft University of.

D'Amico, S. a. (2006). Proximity operations of formation-flying spacecraft using. *Journal of Guidance, Control, and Dynamics, 29*, 554-563. Retrieved 09 14, 2016, from http://dx.doi.org/10.2514/1.15114.

D'Amico, S. a.-S. (2013, Jan). Autonomous formation flying based on GPS PRISMA flight results. *Acta Astronautica, 82*, 69--79. Retrieved 09 14, 2016, from http://dx.doi.org/10.1016/j.actaastro.2012.04.03

Gurfil, M.-P. R. (2008, Dec). Precise Spacecraft Relative Positioning using Single-Frequency Pseudorange Measurements. *Journal of Navigation, 62*, 119. Retrieved 09 14, 2016, from http://dx.doi.org/10.1017/S0373463308005006

Hueso González, J., Walter Antony, J. M., Bachmann, M., Krieger, G., Zink, M., Schrank, D., & Schwerdt, M. (2012). Bistatic system and baseline calibration in TanDEM-X to ensure the global. (Elsevier, Ed.) *ISPRS Journal of Photogrammetry and Remote Sensing, 73*(3-11), pp. 1-11.

Hunger, R. (2007). *Floating point operations in matrix-vector calculus.* München, Germany: Munich Univ. of Technology, Inst. for Circuit Theory and Signal Processing.

Jäggi, A., Montenbruck, O., Moon, Y., Wermuth, M., König, R., Michalak, G., . . . Bodenmann, D. (2012). Inter-agency comparison of TanDEM-X baseline solutions. (Elsevier, Ed.) *Advances in Space Research, 50*, pp. 260-271.

JPEG 2000. (2016, 07 15). (Université de Louvain (UCL), Belgium) Retrieved 08 19, 2016, from http://www.openjpeg.org/

Ju, Z. L. (2009). Precise relative positioning of formation of spacecraft using GPS. *International Conference on Space Information Technology.* Intl Soc Optical Eng. Retrieved 09 14, 2016, from http://dx.doi.org/10.1117/12.855923

Klimesh, M. (2005). *Low-complexity lossless compression of hyperspectral imagery via adaptive filtering.* NASA-JPL.

Klimesh, M. (2005). *Low-complexity lossless compression of hyperspectral imagery via adaptive filtering.* NASA-JPL.

Krieger, G., Moreira, A., Fiedler, H., Hajnsek, I., Werner, M., Younis, M., & Zink, M. (2007, 11 11). TanDEM-x: A Satellite Formation for High Resolution SAR Interferometry. *IEEE Transactions on Geoscience and Remote Sensing*, pp. 3317-3341.

Lopez, G., Napoli, E., & Strollo, A. G. (2015). FPGA implementation of the CCSDS-123.0-B-1 lossless Hyperspectral Image compression algorithm prediction stage. *IEEE 6th Latin American Symposium on Circuits & Systems (LASCAS),*, (pp. 1-4).

Montenbruck, S. D. (2006). Relative Orbit Control Design for the PRISMA Formation Flying Mission. *AIAA Guidance, Navigation, and Control Conference and Exhibit.* American Institute of Aeronautics and Astronautics AIAA. Retrieved 09 14, 2016, from http://dx.doi.org/10.2514/6.2006-6067

Moreira, A. K. (2004). TanDEM-X: a TerraSAR-X add-on satellite for single-pass SAR interferometry. *Geoscience and Remote Sensing Symposium. 2*, pp. 1000-1003. IEEE International. Retrieved 09 14, 2016, from http://dx.doi.org/10.1109/IGARSS.2004.1368578

Nian, Y., Xu, K., Wan, J., Wang, L., & He, M. (2016). Block-based KLT compression for multispectral images. *International Journal of Wavelets, Multiresolution and Information Processing, 14*(04).

Reigber, A., Alivizatos, E., Potsis, A., & Moreira, A. (2006, June). Extended wavenumber-domain synthetic aperture radar focusing with integrated motion compensation. *IEE Proc.-Radar Sonar Navig, 153*(3), pp. 301-310.

Rodriguez-Cassola, M., Prats, P., Schulze, D., Tous-Ramon, N., Steinbrecher, U., Marrotti, L., . . . Moreira, A. (2012, Jan). First Bistatic Spaceborne SAR Experiments with TanDEM-X. *EEE Geoscience and Remote Sensing Letters, 9*(1), pp. 33-37. Retrieved 09 14, 2016, from http://dx.doi.org/10.1109/LGRS.2011.2158984

Santos, L., Berrojo, L., Moreno, J., J., & López, J. F. (2016). Multispectral and Hyperspectral Lossless Compressor for Space Applications (HyLoC): A Low-Complexity FPGA Implementation of the CCSDS 123 Standard. . *IEEE Journal of Selected Topics in Appliad Earth Observation and Remote Sensing, 9*(2), pp. 757-770.

Thompson, D. R., Green, R. O., Keymeulen, D., Lundeen, S. K., Mouradi, Y., Nunes, D., & Chien, S. (2014). (2014). Rapid spectral cloud screening onboard aircraft and spacecraft.,, . *IEEE Transactions on Geoscience and Remote Sensing, 52*(11), pp. 6779-6792.

Torres, R., Snoeij, P., Geudtner, D., Bibby, D., Davidson, M., Attema, E., . . . Brown , M. (2012, May 15). GMES Sentinel-1 mission. *Remote Sensing of Environment*, pp. 9–24.

Vandewal , M., Speck, R., & Süß, H. (2007). Efficient and Precise Processing for Squinted Spotlight SAR through a Modified Stolt Mapping. *EURASIP Journal on Advances in Signal Processing*.

Villano, M., Krieger, G., & Moreira, A. (2014.). Staggered SAR: High-Resolution Wide-Swath Imaging by Continuous PRI Variation. *IEEE Transactions on Geoscience and Remote Sensing, 52*(7), 4462-4479.

Walter Antony, J. M., Hueso González, J., Schwerdt, M., Bachmann, M., Krieger, G., & Zink, M. (2013, June). Results of the TanDEM-X Baseline Calibration. *IEEE Journal of Selected Topics in Applied Earth Observations and Remote Sensing, 6*(3), pp. 1495-1501.

Wermuth, M., König, R., Moon, Y., Walter Antony, J. M., & Montenbruck, O. (2014, March 26). Two years of TanDEM-X baseline determination. (InderScience, Ed.) *International Journal of Space Science and Engineering*, pp. 1-13.

Yu, G., Vladimirova, T., & Sweeting, M. (2007). Autonomous band registration for on-board applications. *ICSPC - International Conference on Signal Processing and Communications* (pp. 1327-1330). IEEE.

Yu, G., Vladimirova, T., & Sweeting, M. (2007, July). A new automatic on-board multispectral image compression system for Leo Earth observation satellites. *15th International Conference on Digital Signal Processing* (pp. 395-398). IEEE.

Yu, G., Vladimirova, T., & Sweeting, M. (2007, November). Autonomous band registration for on-board applications. *ICSPC - International Conference on Signal Processing and Communications* (pp. 1327-1330). IEEE.